

Optimized Adaptive Control for the MYRRHA Linear Accelerator


ISAÍAS MARTÍN-HOYO,
FRÉDÉRIC BOULY,
NICOLAS GANDOLFO,
CHRISTOPHE JOLY,
ROCCO PAPARELLA,
JEAN-LUC BIARROTTE, and
JUAN M. MARTÍN-SÁNCHEZ

**CONTROL SYSTEM
DESIGN FOR A
SUPERCONDUCTING
CAVITY IN A PARTICLE
ACCELERATOR**



ALL-FREE-DOWNLOAD.COM

Digital Object Identifier 10.1109/MCS.2017.2786420
Date of publication: 16 March 2018



Energy forecasts indicate that world primary energy consumption will increase significantly (approximately 37%) by 2040, despite projected improvements in energy efficiency. World electricity demand is expected to increase to almost 80% by 2040 [1]. As a result, electricity usage will increase more rapidly than the share of other energies, even more so when carbon-avoiding technologies are implemented. The security of the energy supply is, and will be, a major concern for the world.

The use of nuclear energy must be consistent with sustainable development goals. Besides concern about potential proliferation, there also exists the challenge of raising nuclear safety levels even higher while improving the economic competitiveness of nuclear power. Using technologically reliable and socially acceptable nuclear waste solutions is crucial. At present, the European Union relies on nuclear fission for approximately 25% of its electricity supply, leading to an approximate annual production of 2500 t of used fuel, which contains 25 t of plutonium, 3.5 t of minor actinides (MAs, namely neptunium, americium, and curium), and 3 t of long-lived fission products (LLFPs) [2], [3]. These MA and LLFP stocks must be managed in an appropriate way.

Used-fuel reprocessing followed by geological disposal (burying the waste) or direct geological disposal are the envisaged solutions, depending on national fuel-cycle options and waste-management policies. However, the time scale presently considered for geological disposal is not publicly accepted and exceeds what may be accomplished by current technological knowledge. In addition, radiotoxic nuclear waste generates a significant amount of heat, which directly impacts the size of deep geological repositories. The maximum density of nuclear waste that can be stored is limited by the thermal load that the geological soil can support [4].

In an attempt to address these concerns, [5]–[7] identify the adequate separation of nuclear waste, referred to as partitioning, and the transmutation of some of them (MAs and LLFPs) as the strategy of choice to relax time constraints on geological disposal (from 200,000 to 2 million years) to technologically relevant and manageable time scales (~250 years).

The Preliminary Design Studies of an eXperimental Accelerator-Driven System (PDS-XADS) [8] is a European-funded project that served as the basis for the design of an ADS, which is the reference solution to the transmutation of nuclear waste. Further development toward the demonstration of the ADS transmutation concept was achieved through the European Research Programme for the TRANsmutation of High-Level Nuclear Waste in an ADS (EUROTRANS) project [6]. The project was launched

as part of an integrated effort by the European Commissions Sixth Framework Programme to enhance research on strategic issues. One of the results of EUROTRANS was the preliminary design of an experimental ADS facility to demonstrate and validate the incineration and transmutation of nuclear wastes (MAs and LLFPs).

An ADS consists of a transmutation reactor, containing the nuclear waste to be burned, that is driven by a particle accelerator. The accelerator is a key element in ADS technology. Its function is to generate a high-energy proton beam that collides with a spallation target, thus producing the fast neutrons necessary for the transmutation reaction. The processed fission products and MAs are then converted into shorter radioactive half-life elements.

The Multipurpose Hybrid Research Reactor for High-tech Applications (MYRRHA) is intended to be the first medium-power transmutation reactor (100 MWth) and will be placed in the Belgian nuclear research center in Mol, Belgium. EUROTRANS's outcome preceded the Seventh Framework Programme (FP7) MYRRHA Accelerator eXperiment, Research and Development Program (MAX) project [9], aimed at performing and/or pursuing the component-related research and development to set the design details for the accelerator.

In the operating context of the ADS, and particularly of MYRRHA, the essential role of the accelerator control system can hardly be overemphasized, due to the high reliability requirements. The proton beam is accelerated in a set of superconducting (SC) cavities, in which the precise control of the field amplitude and phase is of paramount importance for obtaining required stability levels in terms of beam power and position on target. SC cavities are nonlinear and time-varying processes, characterized by their optimal operating conditions being at a certain electromagnetic resonance frequency and the necessity of avoiding exciting mechanical resonance modes. However, the resonance frequency is a very sensitive feature that depends on the shape of the SC cavity, which in turn may be modified by the operating conditions and different kinds of stochastic and unmeasured perturbations. Maintaining this resonance frequency at its optimal operating value is critical. Mechanical devices called cold tuning systems (CTSs) driven by piezoelectric actuators were developed for this purpose. The control of a CTS presents multiple difficulties that have challenged the research efforts of numerous scientists in the accelerator community [10]–[17].

Due to their control difficulty, SC cavities presented a control scenario suitable for testing the performance of a new adaptive predictive expert (ADEX) control methodology [18], [19] that has already been applied to difficult-to-control processes in the industrial field with excellent results [20]–[23]. ADEX uses adaptive predictive control (APC) [24], [25], including an adaptive self-tuning feature that automatically addresses process and environmental uncertainties and identifies and tracks actual process

Summary

The multipurpose hybrid research reactor for high-tech applications (MYRRHA) is envisaged to be the first midsize, industrial-scale demonstrator of a transmutation reactor for the incineration of nuclear waste. It will be operative in Mol, Belgium, by 2030 and rely on a proton accelerator producing a high-energy beam that initiates and maintains transmutation within the reactor. The resonance frequency of the accelerator's superconducting (SC) cavities is a critical variable that determines the performance and stability of the acceleration process. This article describes the design of an optimized adaptive control system (OACS) based on the adaptive predictive expert control methodology and illustrates its application to the resonance frequency of a high-fidelity SC cavity simulator of the MYRRHA proton linear accelerator developed by the Centre National de la Recherche Scientifique, France. The OACS approach enhanced the stability and control precision of the resonance frequency and proved to be reliable under unforeseen perturbations that had previously caused cavity failure under the operation of one of the most advanced proportional-integral-derivative-based control systems reported in control literature.

dynamics in real time. EUROTRANS recommended that "both standard and ADEX control technologies be thoroughly evaluated as alternative solutions to the ADS control/command system." Therefore, the MAX project conducted experimental evaluation, the results of which are partially presented in this article.

A control strategy for an SC-cavity resonance frequency must consider the associated instrumentation and dynamic nature of the SC cavity. Essential parts of this control system are the filtering and signal processing tools used to avoid exciting the inherent resonance modes and compensate for the externally excited ones.

An optimized adaptive control system (OACS) [26], defined by an optimized control strategy in which ADEX controllers were integrated, was specifically developed for the CTS loop that controls the resonance frequency and was applied to a high-fidelity simulation of the SC cavity provided by the Centre National de la Recherche Scientifique (CNRS) of France. This article presents the OACS design and performance evaluation using the previously mentioned SC cavity simulation. The OACS performance was compared with some of the most significant proportional-integral-derivative (PID) controller-based control systems that were previously applied to the CTS loop [14]–[16]. The favorable evaluation of the OACS performance in simulation has been a significant milestone, mandatory for its implementation in the prototypical cavities currently studied at the Institut de Physique Nucléaire d'Orsay facility of CNRS [27].

The article presents an overview of the MYRRHA ADS principle, its accelerator structure, and operation. Next is a description of the proton-acceleration process that occurs inside an SC cavity, including the principles and challenges of the cavity control loops [namely, the low-level radio frequency (LLRF) and CTS loops] that must be considered to achieve a proper acceleration of the beam. As explained in "Summary," the article then discusses previous advanced control systems based on PID controllers for the CTS loop and presents the basic concepts of OACS and the AP algorithms used for the CTS loop in the context of ADEX methodology. The final sections describe how the optimized control strategy is applied, shows the results obtained by the OACS when applied to a simulation of the cavity, and compares them to those obtained by some of the PID-based control systems.

THE MYRRHA ADS AND ITS ACCELERATOR

The ADS Concept

An ADS is a hybrid nuclear fission reactor, driven by a particle accelerator. Unlike conventional critical reactors where the neutron population is sufficient to self-sustain the nuclear reaction, the subcritical core of an ADS requires an external neutron source to maintain the reactor operation. These additional neutrons are provided by a high-energy proton accelerator. The protons hit a specific target and produce neutrons by the spallation process [28]. ADS devices are considered a potential solution to reduce the volume and radiotoxicity of the accumulated nuclear waste, in particular MA and LLFPs [29]. Nuclear waste reduction can be achieved by transmutation and fission of these wastes under a high neutron flux [30].

The MYRRHA project, initiated by SCK-CEN, aims to construct a new nuclear facility in Mol [31]. This large-scale reactor prototype is designed to demonstrate the ADS concept for the transmutation of high-level radioactive waste (see Figure 1). The MYRRHA subcritical core will be cooled by a lead-bismuth eutectic (LBE). The LBE will also be used in the spallation target to produce the necessary neutron flux to operate the reactor. The facility therefore requires a continuous wave proton beam with a maximum power of 2.4 MW (600 MeV–4 mA).

In addition to providing a megawatt proton beam, the high-power accelerator must be extremely versatile to fulfill the exceptionally high level of reliability required to operate the ADS. Indeed, frequently repeated beam interruptions can induce high thermal stresses and fatigue on the reactor structures, the target, or the fuel elements. Moreover, beam interruptions will probably be systematically associated with reactor shutdowns that may also significantly affect the availability of the system, since the considered restart procedures could typically last about 20 h [32].

Thus, the number of beam interruptions must remain extremely low. The present tentative limit is ten beam

ADS devices are considered a potential solution to reduce the volume and radiotoxicity of the accumulated nuclear waste.

interruptions, longer than 3 s, per three-month operating cycle [33]. This leads to a global accelerator mean time between failures of approximately 250 h, which is a new and challenging goal in the field of high-power accelerators.

To address these requirements, the MYRRHA accelerator is based on a *linac* solution, mainly composed of accelerating SC cavities. The linac structure was established with redundant elements to enable failure mitigation (namely cavity failures) of fewer than 3 s during operation.

The Proton Accelerator

Main Linac Characteristics

The present conceptual design of the ADS-type proton accelerator was initiated through previous European Atomic

Energy Community (EURATOM) Framework Programmes: PDS-XADS and EUROTRANS projects. It has been consolidated in the frame of the MAX project (EURATOM FP7) [34]. The conceptual scheme of the accelerator is given in Figure 2; it is composed of an SC linac and an injector that preaccelerates protons to a kinetic energy of 17 MeV [35], [36]. The injector is a compact, accelerating line that is approximately 20 m long. The best way to compensate failures in the injector is to double the line; a second hot, standby, spare injector is provided to quickly resume beam operation in case of failure in the main one [37].

From the injector, the beam is then accelerated through the 17-600 MeV main linac, which is approximately 250 m long. The accelerator is composed of three sections with different cavity families, whose main characteristics are

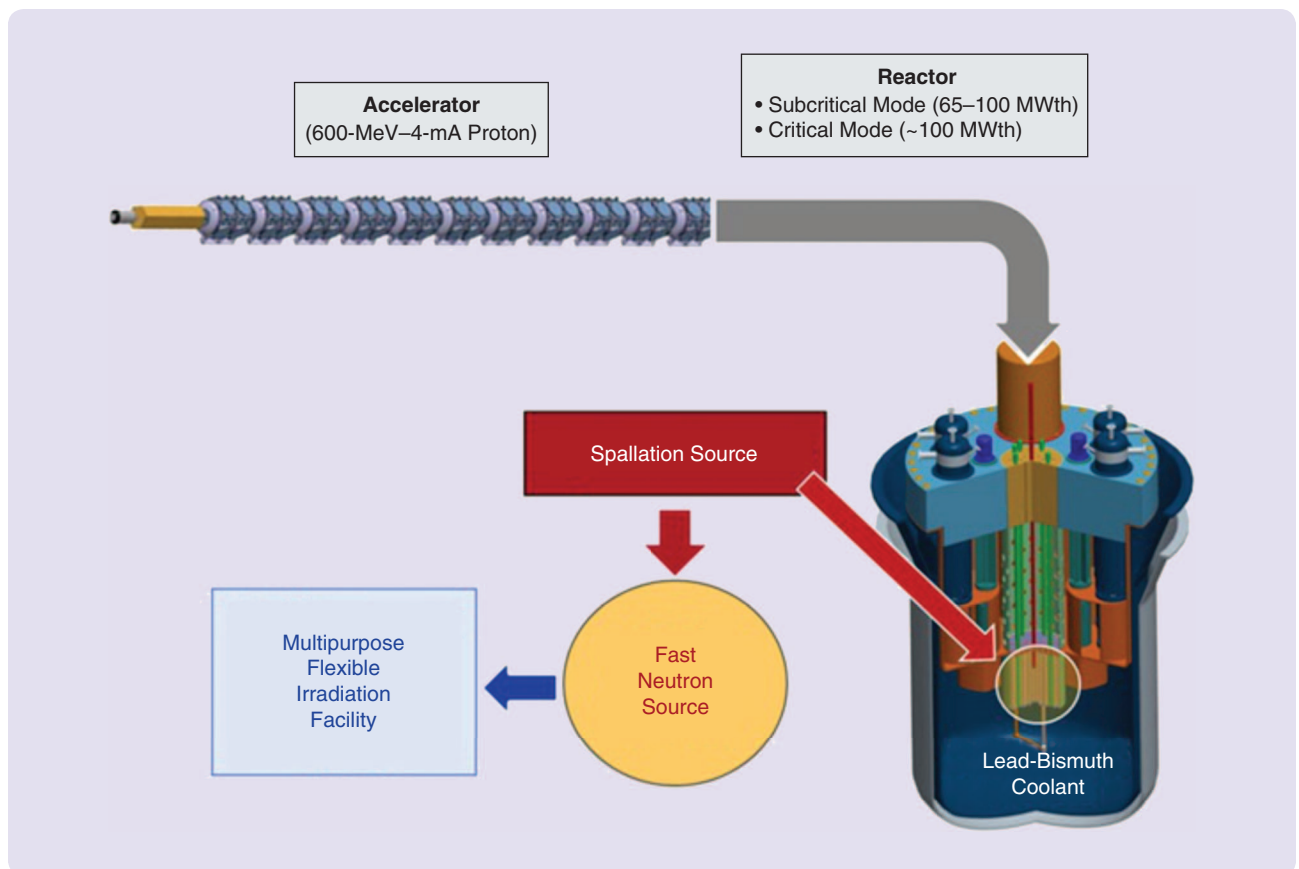


FIGURE 1 The scheme and main characteristics of the Multipurpose Hybrid Research Reactor for High-tech Applications Accelerator Driven System (MYRRHA ADS). MYRRHA ADS is a fission reactor, piloted by the proton beam, delivered by a linear accelerator, and targeting a spallation source in the reactor core. The high-energy proton beam impacting the spallation source will produce fast neutrons for research purposes. One of the main objectives is to demonstrate the industrial feasibility of nuclear waste transmutation. (Image used courtesy of SCK-CEN.)

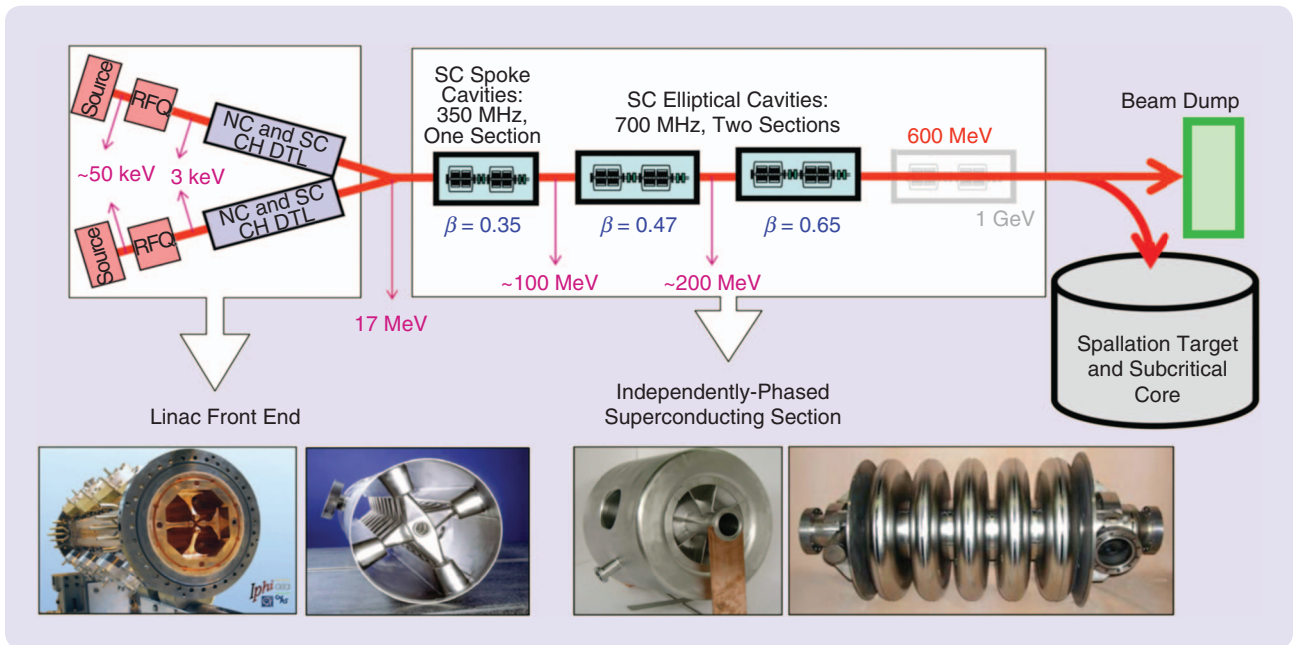


FIGURE 2 The accelerator driven system accelerator conceptual scheme. The accelerator is mainly composed of a linac front end, or injector, which delivers a proton beam at 17 MeV to a superconducting section, or main linac, which accelerates this beam up to 600 MeV. (Image used courtesy of Institut de Physique Nucléaire d'Orsay.)

Table 1 The main characteristics of the linac cavities [40]. These cavities have been designed regarding specific reliability guidelines for the MYRRHA linac. The goal is to provide a stable and robust beam with operational margins and allow maximum redundant elements for failure mitigation. *The optimal β , β_{opt} , is the β (velocity) for which the acceleration is the most efficient in the cavity; that is, highest E_{acc} . **The accelerating field E_{acc} is given at optimal β and normalized to $L_{acc} = N_{gap}\beta_{opt}\lambda/2$.

Section number	Number 1	Number 2	Number 3
E_{input} (MeV)	17.0	80.8	184.2
E_{output} (MeV)	80.8	184.2	600.0
Cavity technology	Spoke	Elliptical	
Resonance frequency (MHz)	352.2	704.4	704.4
Optimal β *	0.375	0.510	0.705
Cells per cavity	2	5	5
E_{accNom} ** (MV/m)	6.4	8.2	11.0
E_{accMax} ** (MV/m)	8.3	10.7	14.3
Number of cavity/ cryomodule	2	2	4
Total number of cavities	48	34	60
Synchronous phase ($^{\circ}$)	-40 to -18	-36 to -15	
Beam power load/cavity (kW)	1.5 to 8	2 to 17	17 to 32
Section length (m)	73.0	63.9	100.8

given in Table 1. The first section regroups spoke cavities [38], and the two following sections are composed of two different types of five-cell elliptical cavities [39]. Each cavity provides an electric field along the beam axis that enables particle acceleration. All of the cavities will be made of niobium, which is an SC material below a temperature of ~ 9.2 K. To optimize the power transmission efficiency, from cavities to the beam, the temperature must be kept at ~ 2 K. The cavities are therefore regrouped in cryogenic vessels, called cryomodules. All choices for the linac design result from beam physics studies, which are detailed in [40]. The reliability guidelines are a key aspect in the MYRRHA linac design.

Fault Compensation in the Linac

Unlike the injector, the fault compensation scheme in the main linac is based on serial redundancy. The currently adopted strategy is to use a local compensation method (see Figure 3) to compensate for failures of cavities, their associated control systems, and their power supply. As shown in Figure 3, a cavity fault is compensated by acting on the accelerating gradient and the phase of the four nearest-neighboring cavities operating derated (that is, not already used for compensation). The beam is turned off during this retuning procedure. Therefore, the retuning procedure must be sufficiently fast to resume the beam in fewer than 3 s, so the beam interruption remains “transparent” for the ADS operation.

This retuning scheme can only be achieved by providing significant power and accelerating gradient overhead throughout the three SC sections. As a consequence, the

operating accelerating gradients of the MYRRHA cavities have been chosen on the conservative side. To enable the compensation procedures under nominal conditions, the cavities operate with an accelerating gradient that is 30% below its maximum capabilities [40]–[42]. Beam physics studies have been carried out to evaluate the feasibility of the retuning procedures. The results obtained tend to show that it is possible to apply the local compensation method without substantially perturbing the beam transport and acceleration [43].

The following section describes the operating principle of SC cavities and the control loops that are critical to provide proper beam acceleration. The adopted global control strategy for the cavities of the MYRRHA linac will then be discussed.

ACCELERATION PROCESS IN A CAVITY AND CONTROL LOOPS

Accelerating Cavity

Principle and Synchronism Condition

An accelerating cavity is an RF resonator that enables the storage of an electromagnetic wave, whose frequency belongs to a bandpass around the cavity's intrinsic resonance frequency, by reflecting this wave on the cavity walls. Figure 4 shows an example of a five-cell elliptical cavity of the MYRRHA linac section #2; the cavity prototype built by Istituto Nazionale di Fisica Nucleare di Milano [44] is shown in (a), and (b) features the vector electric field in the cavity together with the sketch (in red) of a particle bunch in

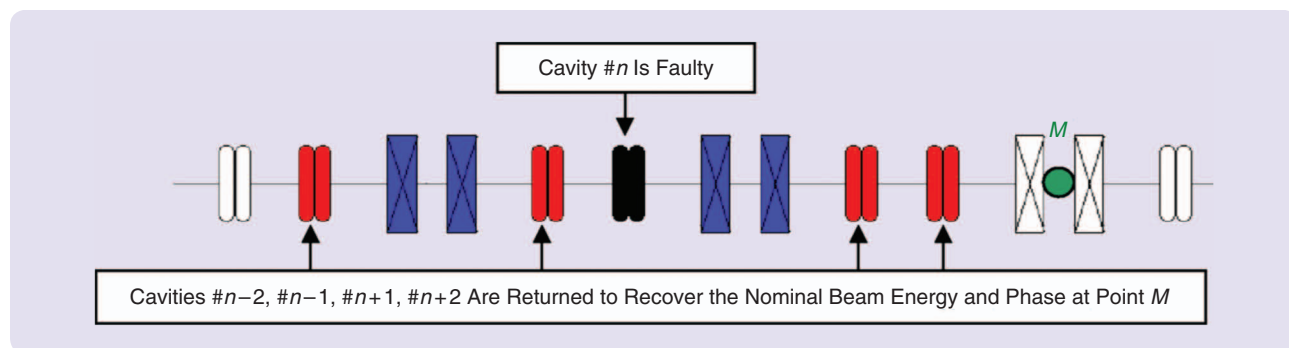


FIGURE 3 The principle of the local compensation method in the main superconducting linac [41]. A cavity faulty is compensated by acting on the accelerating gradient and the phase of the four nearest-neighbor cavities operating derated, that is, not already used for compensation. (Image courtesy of the Institut de Physique Nucléaire d'Orsay.)

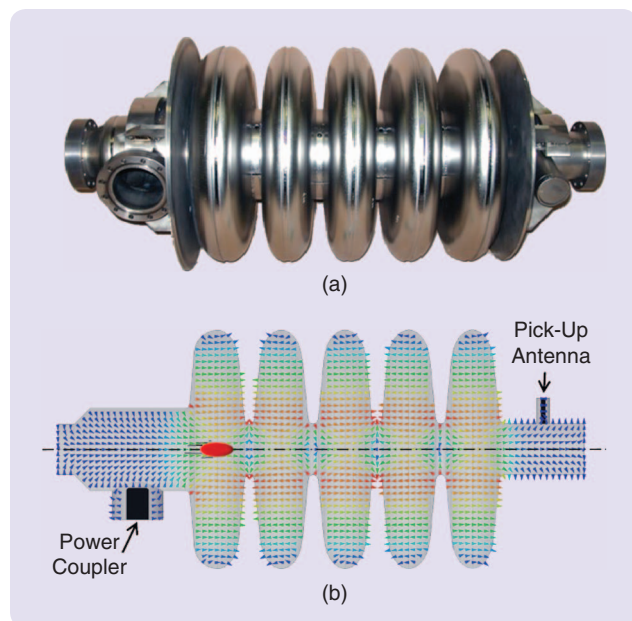


FIGURE 4 A five-cell elliptical cavity: electric field, bunch of particles, and prototype. (a) A cavity prototype for the accelerator [44] and (b) a representation of the vector electric field inside the cavity induced by the power coupler and measured by the pick-up antenna; a particle bunch is depicted in the first cell.

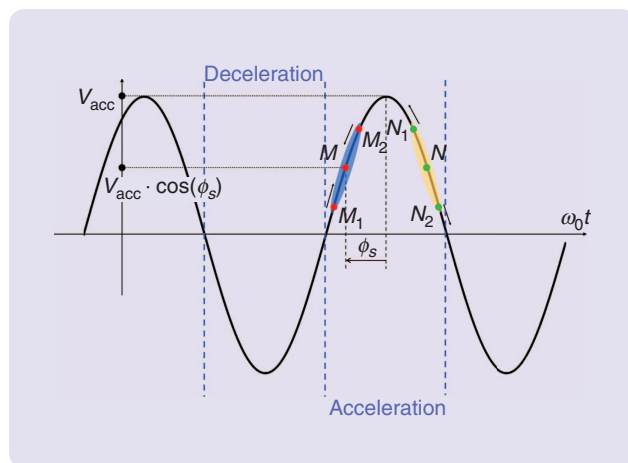


FIGURE 5 An acceleration synchronism. The bunch has a longitudinal spread that characterizes the phase dispersion of the particles. To maintain the cohesion of the bunch throughout its acceleration, it is preferable that the bunch enters the cavity while the field is increasing. Therefore, a particle of the bunch arriving early (M_1) will be accelerated less so it will “wait” for the incoming particles at the end of the bunch (M_2), which will be affected by a higher accelerating field. On the other hand, a bunch arriving in the cavity while the field is decreasing will tend to spread and dilute (N, N_1, N_2). By convention, we consider a synchronous particle (N, M) that represents the bunch average.

Accelerating Field and Main Characteristics

To better understand how the electric field of the RF wave enables the particle acceleration, consider a particle of charge q with velocity $v = \beta c$. This particle enters the cavity at time $t = t_0$ ($z = 0$) and exits the cavity at t_1 . The energy gain is the work of the electric force on the particle

$$\Delta W = \int_{t_0}^{t_1} q \vec{E} \vec{v} dt, \quad (S1)$$

and \vec{E} is the electric field seen by the particle along the beam axis. The field profile along the beam axis $E_z(z, r = 0)$ depends on the position, and it oscillates at the angular frequency ω_0 . Therefore, the energy gain of a particle, which enters the cavity with a phase shift φ with respect to the RF signal, is

$$\Delta W = q \Re \left[\int_{t_0}^{t_1} E_z(z, r = 0) e^{j(\omega_0 t + \varphi)} v dt \right]. \quad (S2)$$

For one cavity, the energy gain is generally considered small with respect to the kinetic energy of the particle. In this approximation, β is almost constant and (S2) can be simplified as

$$\Delta W = q \Re \left[\int_0^{L_{\text{tot}}} E_z(z, r = 0) e^{j\left(\frac{\omega_0 z}{\beta c} + \varphi\right)} dz \right], \quad (S3)$$

with L_{tot} the total length of the cavity. As a consequence, by identification with (1),

$$V_{\text{acc}} = \frac{|\Delta W|}{q} = \left| \int_0^{L_{\text{tot}}} E_z(z, r = 0) e^{j\frac{\omega_0 z}{\beta c}} dz \right| \quad (S4)$$

and

$$\phi_s = \arctan \left(\frac{\int_0^{L_{\text{tot}}} E_z(z, r = 0) \sin\left(\frac{\omega_0 z}{\beta c} + \varphi\right) dz}{\int_0^{L_{\text{tot}}} E_z(z, r = 0) \cos\left(\frac{\omega_0 z}{\beta c} + \varphi\right) dz} \right). \quad (S5)$$

Finally, by convention, the accelerating field seen by the particle during its travel through the cavity is defined as

$$E_{\text{acc}} = \frac{V_{\text{acc}}}{L_{\text{acc}}} = \frac{1}{L_{\text{acc}}} \left| \int_0^{L_{\text{tot}}} E_z(z, r = 0) e^{j\frac{\omega_0 z}{\beta c}} dz \right|, \quad (S6)$$

with L_{acc} the acceleration length corresponding to the length of the accelerating gaps in a cavity. For example, the elliptical cavity of Figure 4 has five cells, so five accelerating gaps, and $L_{\text{acc}} = 5 L_{\text{cell}}$, while L_{tot} also includes the lengths of the beam tubes.

It can be seen from (S6) that the accelerating field value is directly linked to the velocity of the accelerated particle. It also depends on the amplitude of $E_z(z, r = 0)$, which depends on the RF power that can be stored in the cavity. The maximum power that can be stored will be directly linked to the dissipations of the RF waves on the inner cavity walls. These dissipations are quantified by the quality factor Q_0 for the resonant mode of angular frequency ω_0 , as the ratio between the energy stored U (in joules) and the power dissipated per RF cycle P_{cav} (in watts)

$$Q_0 = 2\pi \frac{\text{Stored energy in the cavity}}{\text{Dissipated energy per RF cycle}} = \omega_0 \frac{U}{P_{\text{cav}}}. \quad (S7)$$

THE CAVITY: A BANDPASS RESONATOR

Due to its geometry, an accelerating cavity enables the storage of an electromagnetic wave that resonates at a given frequency. It is a bandpass resonator, and its behavior is similar to a parallel RLC electrical circuit. In this analogy, the power dissipated in the cavity walls P_{cav} can be expressed as a function of an impedance r_{shunt} subjected to a voltage V_{acc}

$$r_{\text{shunt}} = \frac{V_{\text{acc}}^2}{2P_{\text{cav}}}. \quad (S8)$$

This “shunt impedance” (in ohms) will be as high as the RF losses will be low. In a manner similar to that of the quality factor, r_{shunt} enables quantification of the RF losses in the cavity. It is, therefore, interesting to link those two parameters with their ratio (r/Q). According to (S6)–(S8),

$$\left(\frac{r}{Q} \right) = \frac{(E_{\text{acc}} L_{\text{acc}})^2}{2\omega_0 U}. \quad (S9)$$

The (r/Q) is a critical parameter, and it must be optimized during the design to maximize cavity performance. The (r/Q)

is along the beam axis and the amplitude of the field is oscillating at the frequency, f_0 , of the injected RF signal.

the first cell. The electromagnetic wave propagates, through wave guides from the radio-frequency (RF) power generator, and is injected into the cavity by an antenna: the power coupler. Another antenna known as the pick-up measures the electromagnetic wave inside the cavity and uses it as a feedback signal for the cavity control loops.

To enable proper acceleration of the beam, the particles are grouped in bunches whose passage through the accelerating gaps must be synchronized with the field oscillations. When accelerating a bunch, the electric field direction

is along the beam axis and the amplitude of the field is oscillating at the frequency, f_0 , of the injected RF signal.

The bunch has a longitudinal spread that characterizes the phase dispersion of the particles. To maintain the cohesion of the bunch throughout its acceleration, it is preferable that the bunch enters into the cavity while the field is rising. This case is shown in Figure 5, which displays the overall acceleration voltage, as seen by a particle passing through the cavity, as a function of its longitudinal position in the bunch. A particle of the bunch arriving a little

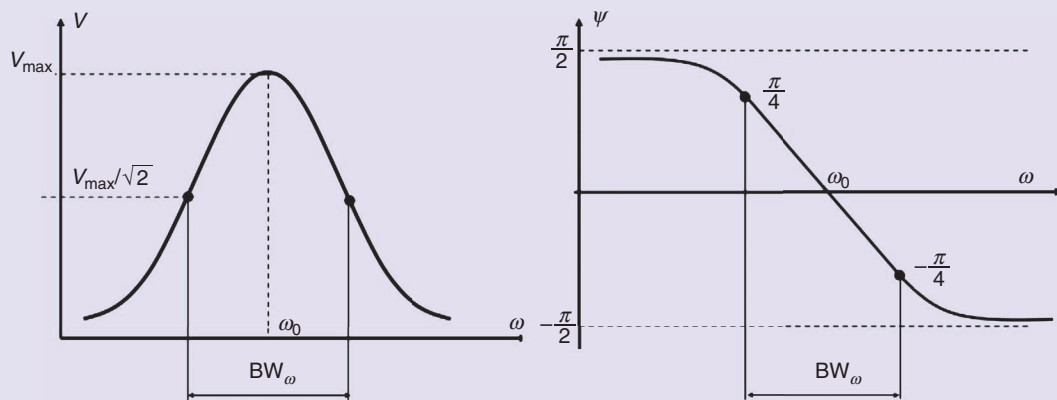


FIGURE S1 A cavity Bode diagram. In the case of a superconducting cavity, the order of magnitude of Q_0 is between 10^9 and 10^{10} , and the loaded quality factor is also rather high: $Q_L \approx 10^7$ depending on the beam properties and the accelerating voltage in the cavity [16]. At these conditions, the bandwidth of the cavity is directly linked to Q_L . In a superconducting linac, such as MYRRHA, the cavities have a very narrow bandwidth, around 100 Hz, which makes them very sensitive to any perturbation.

depends on the geometry of the cavity, but it is also related to E_{acc} . Therefore, for a given stored energy in the cavity, the higher (r/Q) is, the higher E_{acc} will be. In this way, the power losses P_{cav} will be minimized.

Nevertheless, the RF power from the generator is not only dissipated in the cavity, but a major part is absorbed by the beam. Still, there are also significant losses in the power coupler and waveguides, in other words, throughout the external environment of the cavity. As a consequence, an external quality factor (or external coupling) can also be defined that takes into account the losses (P_{ext}) in all the other systems apart from the cavity (such as the power coupler and waveguides)

$$Q_{\text{ext}} = 2\pi \frac{\text{Stored energy in the cavity}}{\text{External dissipated energy per RF cycle}} = \omega_0 \frac{U}{P_{\text{ext}}}. \quad (\text{S10})$$

In the same way, it is possible to define the loaded quality factor (or loaded coupling) of the cavity Q_L , which takes into account the total RF losses

$$Q_L = 2\pi \frac{\text{Stored energy in the cavity}}{\text{Total dissipated energy per RF cycle}} = \omega_0 \frac{U}{P_{\text{cav}} + P_{\text{ext}}} = \omega_0 \frac{U}{P_{\text{tot}}}. \quad (\text{S11})$$

In the case of a superconducting (SC) cavity, the order of magnitude of Q_0 is between 10^9 and 10^{10} , and the loaded quality factor is also rather high: $Q_L \approx 10^7$ depending on the beam properties and accelerating voltage in the cavity [16]. Under these conditions, the bandwidth of the cavity is directly linked to Q_L (see Figure S1) [S1]

$$BW_\omega \approx \frac{\omega_0}{Q_L} \Leftrightarrow BW_f \approx \frac{f_0}{Q_L}. \quad (\text{S12})$$

In an SC linac, such as MYRRHA, the cavities have a very narrow bandwidth (around 100 Hz), which makes them very sensitive to any perturbation.

REFERENCE

[S1] T. Schilcher. (1998). Vector sum control of pulsed accelerating fields in Lorentz force detuned superconducting cavities. Ph.D. dissertation, DESY. [Online]. Available: <https://bib-pubdb1.desy.de/record/291638/files/schilcher.pdf>

too early (M_1) will be accelerated less, so it will tend to wait for the incoming particles at the end of the bunch (M_2), which will be affected by a higher accelerating field. On the other hand, a bunch arriving in the cavity while the field is decreasing will tend to spread and dilute (N, N_1, N_2).

By convention, an “ideal” particle is one that enters neither too early nor too late in the cavity. This reference particle is called the synchronous particle, and it enables the definition of an equilibrium phase that guarantees the synchronism condition between the accelerating wave and the bunch. This

synchronous phase ϕ_s can be understood as the average phase of the bunch with regard to the RF wave, during its travel through the cavity. For details, see “Accelerating Field and Main Characteristics.” Thus, considering the particles charge q the energy gain of the beam can be modeled as

$$\Delta W = q V_{\text{acc}} \cos(\phi_s), \quad (1)$$

where V_{acc} is the maximal possible accelerating voltage. The synchronous phase choice, for each cavity, is dictated

by the beam physics, to guarantee good acceleration of the beam without losing particles.

Detuning of Resonance Frequency by Perturbations

During normal operation, the resonance frequency of the cavity must be maintained very close to the frequency of the RF signal injected into the cavity. The RF signal frequency from the generator is constant and equal to the frequency (or a harmonic) of the repetition rate of the bunches passing through the cavity. It is essential to maintain the accelerating field at a constant value to enable good acceleration of the beam bunches. However, a change in the resonance frequency of the cavity will induce a modification of phase ψ , meaning a change of phase between the input RF signal, injected with the power coupler, and the output RF signal from the pick-up antenna. This also results in a modification of the synchronous phase ϕ_s , the phase between the beam and the accelerating field. As a consequence, the energy gain is modified in the cavity, and the acceleration process is perturbed. This mechanism is described in Figure 6. At time t_0 , the resonance frequency of the cavity (f_{cav}) is equal to the frequency of the injected signal (f_{RF}). At time t_1 , the resonance frequency has changed due to mechanical perturbations on the cavity. Consequently, the accelerating voltage decreases, and the phase is modified. To keep the same accelerating field in the cavity, it is necessary to increase the amplitude and adjust the phase of the injected RF signal. The control of the phase and the amplitude is achieved with the LLRF feedback loop. Nevertheless, these changes will induce a power over-consumption and may lead to the saturation of the RF power amplifier [16].

As a consequence, it is necessary to control the mechanical deformations of the cavity. The principle of the mechanical tuning system, on which the studies presented in this article are based, will be explained in the following

sections. It was designed and built to compensate for, at best, the main mechanical perturbations of different types.

» *The Lorentz forces:* The electromagnetic signal stored inside the cavity induces radiation pressure on its walls. This results in a small deformation of the cavity, resulting in a resonance frequency detuning [45]. The accelerating field inside a cavity E_{acc} can be defined from the accelerating voltage as

$$E_{\text{acc}} = \frac{V_{\text{acc}}}{L_{\text{acc}}}, \quad (2)$$

where L_{acc} is the accelerating length. The static detuning Δf_L can be expressed as a function of the accelerating field E_{acc} and the Lorentz factor k_L . The Lorentz factor can be estimated with mechanical and electromagnetic simulations. It can also be measured during cavity tests, and is given in Hz/(MV/m)². The static detuning amplitude due to Lorentz forces increases with the square of E_{acc}

$$\Delta f_L = -k_L E_{\text{acc}}^2. \quad (3)$$

» *The microphonics:* Vibrations due to the environmental systems of the cavity can excite its mechanical modes and create some dynamic detuning. They are barely predictable and can become very critical for the cavity control. In general, the frequency range for microphonics is from ~1 Hz to ~1 kHz. Beyond that range, vibrations are damped by the mechanical elements. The total perturbations due to microphonics is

$$\Delta f_{\text{mic}} = \sum_i \Delta f_i(t) \sin(\omega_i t), \quad (4)$$

with ω_i the angular frequency of the mechanical excitation and Δf_i the detuning amplitude the cavity resonance frequency.

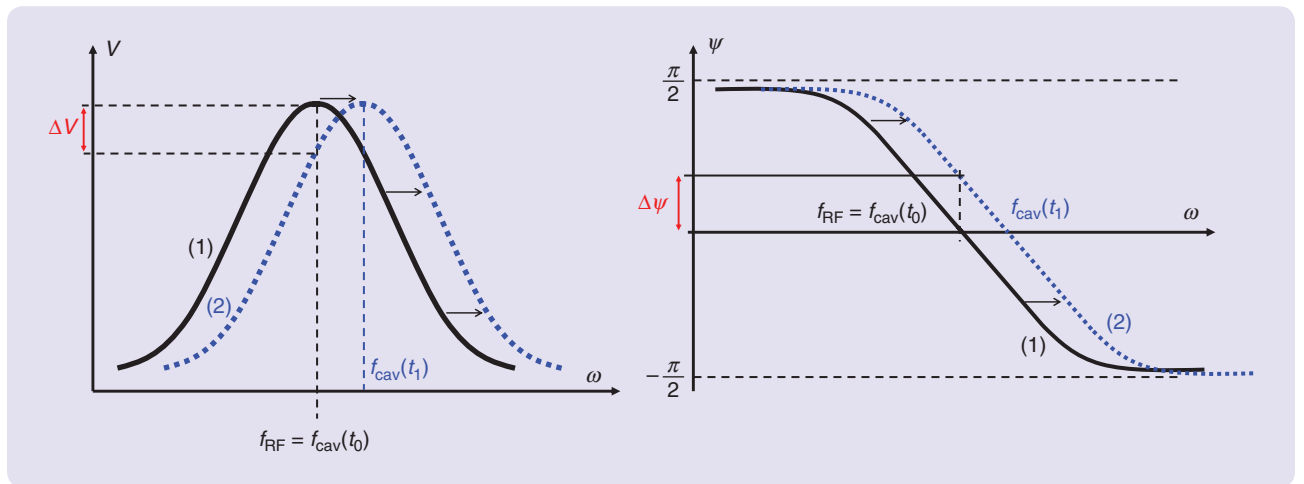


FIGURE 6 The principle of cavity detuning. When the resonance frequency of the cavity changes, the amplitude and phase of the radio frequency (RF) signal are affected. The change must be compensated by increasing the amplitude by ΔV and changing the phase by $-\Delta\psi$.

» *The helium bath:* Some detuning can also be observed due to variations in the helium bath pressure Δf_{He} . Nevertheless, these variations are very slow. The order of magnitude for such time variations is from a few seconds to minutes.

The total detuning of the cavity is

$$\Delta f = f_0 - f_{\text{cav}}, \quad (5)$$

with f_0 the frequency of the injected RF signal in the cavity. The resonance frequency of the cavity, due to detunings, is f_{cav} . Finally, the total detuning of the cavity can be written as

$$\Delta f = -\Delta f_L - \Delta f_{\text{mic}} - \Delta f_{\text{He}} - \Delta f_{\text{CTS}}. \quad (6)$$

In (6), Δf_{CTS} is the contribution of the CTS, which enables compensation for the perturbations. It enables the cavity to be tuned to its optimal frequency detuning $\Delta f_{\text{opt}} = f_0 - f_{\text{cav}}^{\text{opt}}$, to minimize the RF power consumption. The value of Δf_{opt} is not obviously equal to zero and can be expressed from the power balance on the cavity. For details, see “Optimal Frequency Detuning.”

LLRF and CTS Loops

Since power consumption should not exceed reasonable limits, the resonance frequency of each cavity must be kept

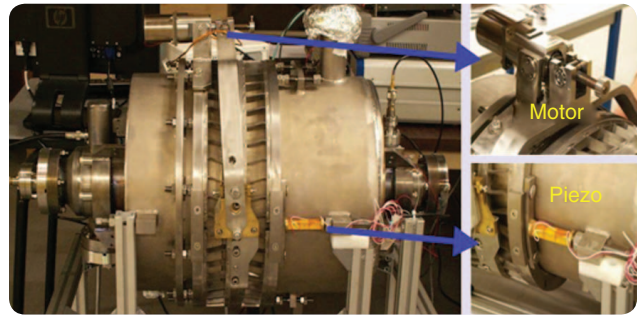


FIGURE 7 A cold tuning system (CTS). The CTS is a mechanical system driven either by a stepper motor or a piezoelectric actuator. The motor or the piezoelectric will induce mechanical efforts on determined points of the CTS. These efforts will be transferred through the CTS to the cavity walls, compressing or expanding them and modifying the resonance frequency [39]. (Image courtesy of the Institut de Physique Nucléaire d'Orsay.)

under control. The resonance frequency of the cavity will be controlled by acting on the CTS. The CTS is a mechanical system able to compress or expand the cavity walls when driven by the stepper motor or by piezoelectric actuators [39]. An example of a CTS implemented in a cryomodule can be seen in Figure 7. Therefore, the control strategy for the cavities of MYRRHA is to use two feedback control loops, as described in Figure 8.

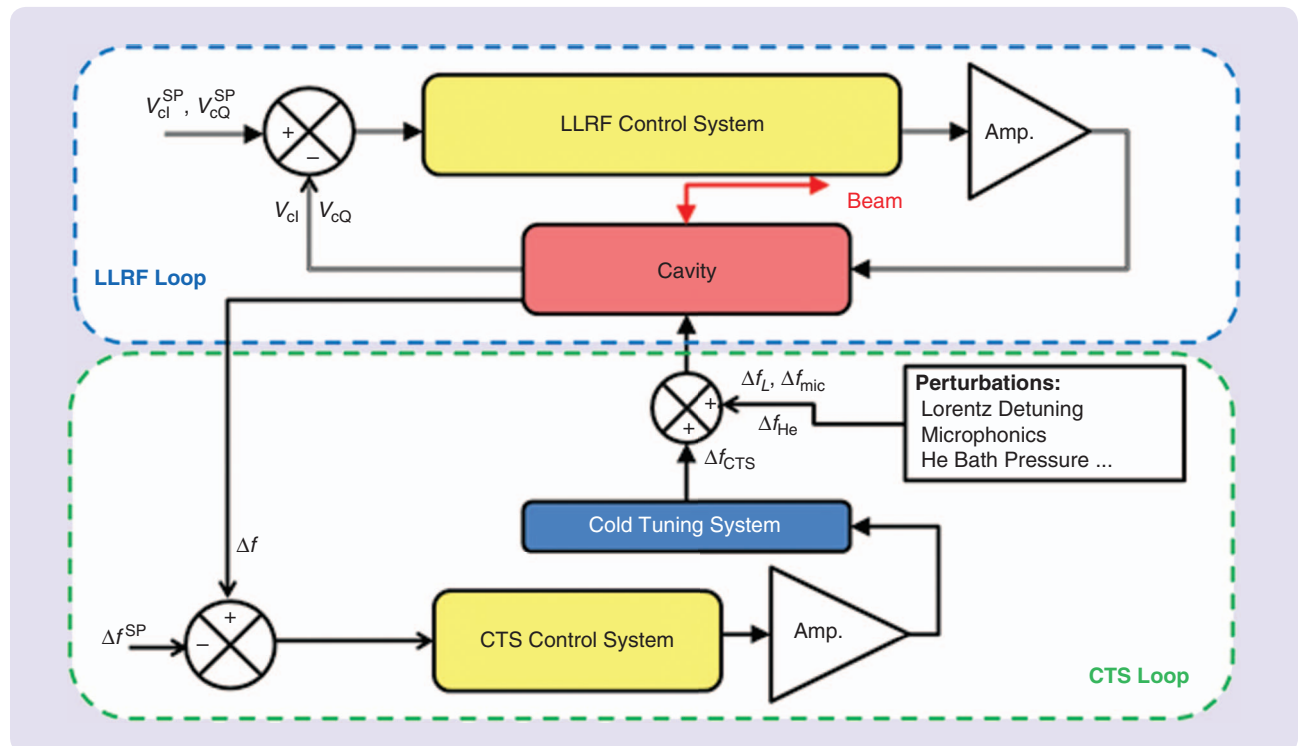


FIGURE 8 The cavity control system strategy. The strategy for cavity control considers two independent control systems, one for the low-level radio frequency (LLRF) loop and another for the cold tuning system (CTS) loop. The LLRF loop maintains the phase (ϕ_s) and amplitude of the field (E_{acc}), measured inside the cavity at their setpoints. The CTS loop maintains the resonance frequency detuning of the cavity (Δf) as close as possible to its optimum value (Δf^{SP}) by acting on the voltage applied to the piezoelectric actuator via the amplifier (amps).

Optimal Frequency Detuning

For a superconducting (SC) cavity (with $Q_0 \gg Q_L$) at steady state (that is, when the accelerating field has been ramped up to a stable value), the power from the generator P_g , the power stored in the cavity P_{cav} , the power transmitted to the beam P_b , and the reflected power at the power coupler port P_{ref} can be written as [16, S1]

$$\begin{cases} P_g = \frac{V_{acc}^2}{8(r/Q)Q_L} \left(1 + \left(2Q_L \frac{\Delta f}{f_0} \right)^2 \right) \\ \quad + \frac{I_{b0} V_{acc}}{2} \left(\cos(\phi_s) + \sin(\phi_s) \left(2Q_L \frac{\Delta f}{f_0} \right)^2 \right) + \frac{(r/Q)Q_L}{2} I_{b0}^2, \\ P_{cav} = \frac{1}{2(r/Q)Q_0} V_{acc}^2, \\ P_b = V_{acc} I_{b0} \cos(\phi_s), \\ P_{ref} = \frac{V_{acc}^2}{2(r/Q)} \left[\frac{1}{4Q_L} \left(1 + \left(2Q_L \frac{\Delta f}{f_0} \right)^2 \right) - \frac{1}{Q_0} \right] \\ \quad + I_{b0} V_{acc} \left[\frac{1}{2} \left(\cos(\phi_s) + \sin(\phi_s) 2Q_L \frac{\Delta f}{f_0} \right) - \cos(\phi_s) \right] \\ \quad + \frac{(r/Q)Q_L}{2} I_{b0}^2. \end{cases} \quad (S13)$$

In addition, by ignoring the power in the pick-up antenna,

$$P_g = P_{cav} + P_b + P_{ref}. \quad (S14)$$

Note that the powers P_g and P_{ref} depend on the desired voltage V_{acc} in the cavity, the beam current I_{b0} , synchronous phase ϕ_s , loaded coupling Q_L , and the cavity detuning Δf .

For a given V_{acc} , I_{b0} , and ϕ_s , the power delivered by the generator depends on the cavity detuning. The power transmission of P_g will be optimal while P_{ref} will be minimized. According to (S13), the detuning that minimizes the reflected power is

$$\Delta f_{opt} = -f_0 \frac{I_{b0}(r/Q)}{V_{acc}} \sin(\phi_s). \quad (S15)$$

To illustrate the importance of optimal detuning, consider the example with a cavity of the linac that operates to a nominal accelerating field $E_{acc} = 8.2$ MV/m ($L_{acc} = 0.5$ m) and with a synchronous phase $\phi_s = -25^\circ$. The beam current is $I_{b0} = 4$ mA and $(r/Q) = 80 \Omega$. According to (S15), the cavity optimal detuning, in steady state, is $\Delta f_{opt} \approx 24$ Hz.

To ensure optimal detuning, the tuning system must compensate for the perturbations, in particular the Lorentz forces. In this example, without considering the influence of the microphonics and the helium bath, the contribution of the tuning system must be

$$\Delta f_{CTS} = -\Delta f_{opt} - \Delta f_L(E_{acc} = 8.2 \text{ MV/m}). \quad (S16)$$

P_g , P_{ref} , and P_b (for an SC cavity P_{cav} is small) are plotted in Figure S2 as a function of the accelerating field in the cavity. The cavity frequency is tuned to compensate for the Lorentz forces at the nominal operation point $E_{acc} = 8.2$ MV/m (solid line curves on Figure S2): here $k_L = 10 \text{ Hz}/(\text{MV/m})^2$ and $\Delta f_L(E_{acc} = 8.2 \text{ MV/m}) \approx -538$ Hz. Two settings of static detuning are represented, one with the solid line and another with the dotted line. Initially, the tuning system is set for optimal op-

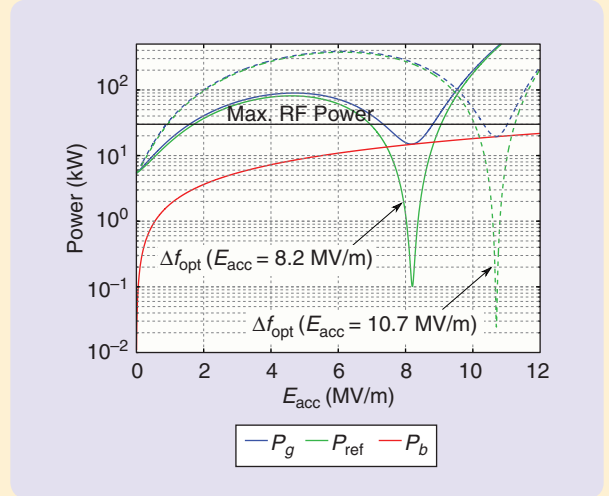


FIGURE S2 The evolution of the generator power P_g , reflected power P_{ref} , and power delivered to the beam P_b as a function of the accelerating field E_{acc} . It is considered that the cavity frequency is tuned to compensate for the Lorentz forces at the nominal operation point $E_{acc} = 8.2$ MV/m (solid curves on Figure S2): here $k_L = 10 \text{ Hz}/(\text{MV/m})^2$ and $\Delta f_L(E_{acc} = 8.2 \text{ MV/m}) \approx -538$ Hz. Two settings of static detuning are represented, one with the solid line and another with the dotted line. Initially, the tuning system is set for an optimal operation at 8.2 MV/m. However, to increase the field value to 10.7 MV/m, the tuning system must move its position to compensate for the Lorentz detuning increase and reach the new Δf_{opt} .

eration at 8.2 MV/m. To increase the field value to 10.7 MV/m, the tuning system has to move its position to compensate for the Lorentz detuning increase and reach the new Δf_{opt} .

The operation is optimal at 8.2 MV/m because the reflected power is minimized. However, around this point, the RF power supply must furnish more power than necessary if the accelerating field has to be changed. In addition, the maximum power (30 kW) that the generator can deliver is quickly reached. As a consequence, if the field has to be increased to 10.7 MV/m (the dashed line curves on Figure S2), it is necessary to reoptimize the frequency detuning of the cavity while the field is ramped up. In this way, the Lorentz detuning is compensated, and there is no power saturation of the generator. When the steady state is reached, the RF power consumption is minimized.

To operate an SC cavity in a continuous-wave mode, it is necessary to use a tuning system that can be dynamically controlled to help the low-level radio frequency feedback loop that enables the stabilization of the accelerating field and phase inside the cavity. The tuning-system control loop must enable the compensation of all the perturbations. The Lorentz forces may bring a high cavity detuning, which leads to power saturation. Microphonics, which may appear randomly, can also strongly perturb the cavity operation. It is, therefore, essential to use a system that can compensate for these dynamic detunings and adapt to their evolutions.

- » *The LLRF loop* maintains the phase (ϕ_s) and the amplitude of the field (E_{acc}) measured inside the cavity at their SPs. In contrast to the traditional amplitude and phase control, the LLRF is based on the control of the real (in phase, V_{cl}) and imaginary (quadrature, V_{cq}) components of the accelerating voltage. It acts on the phase and amplitude of the RF power amplifier signal, injected via the power coupler into the cavity, to maintain the accelerating voltage at its SPs, V_{cl}^{SP} and V_{cq}^{SP} .
- » *The CTS loop* maintains the resonance frequency detuning of the cavity (Δf) as close as possible to its optimum value (Δf^{SP}) by acting on the voltage applied to the piezoelectric actuator via the amplifier (amps). However, the cavity's resonance frequency will be affected by several perturbations such as microphonics or Lorentz detuning (Δf_{mic} and Δf_L , respectively). The CTS control loop must compensate for the effect of these perturbations acting on the CTS, so that it retunes the cavity (Δf_{CTS}).

This article focuses on the CTS loop, its control challenges, which are explained in the following section, and the design of the OACS that will face these challenges.

CTS Loop Main Control Challenges

The CTS loop is a vital part of the acceleration structure. Precise control of the cavity detuning can significantly reduce RF power consumption, which is about 30% of the total amount of energy foreseen for the whole accelerator operation. The main control challenges are as follows.

- » *Dynamics of the cavity resonance frequency.* When driven by piezoelectric actuators, the CTS can also excite some mechanical vibrating modes of the cavity. The dynamic response of the 704.4-MHz, five-cell, elliptical resonance frequency detuning when excited by the piezoelectric actuator was measured and modeled [16]. Figure 9 shows (in blue) the cavity's detuning produced by a sinusoidal excitation with 1-V amplitude on the piezos and frequencies varying from 0 to 1000 Hz. These measurements evaluated the vibrating mechanical modes of the cavity and to model (green curve in Figure 9) the transfer function of the CTS acting on the cavity resonance frequency. It can be seen in Figure 9 that the cavity presents a high number of mechanical resonant modes with different resonant magnitudes. These resonant modes can be excited by the piezoelectric actuator movement or by external vibrations, which might also excite other modes in an unknown manner, producing strong perturbations on the cavity detuning.
- » *Time constraints.* It is well known that the resonance frequency of an operating cavity varies significantly in the range of microseconds/milliseconds. The processing time needed for the OACS execution to perform proper control must be studied with the help of

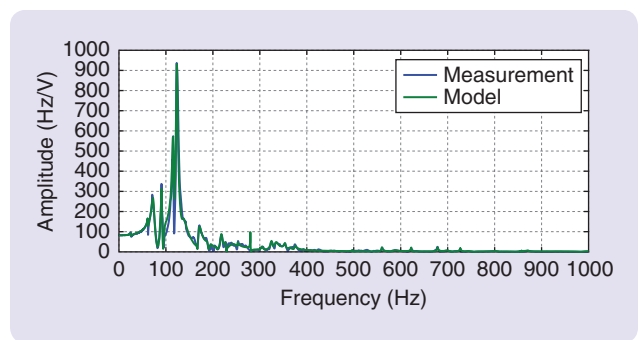


FIGURE 9 Cavity detuning produced by sinusoidal excitations. The detuning is produced due to excitation by different frequency sinusoids of 1-V amplitude applied to the piezoelectrics. The y-axis shows the scale of the amplitude of the resonance frequency detuning, and the x-axis the scale of the frequency of excitation. Four main resonant modes can be observed at 71, 90, 115, and 121 Hz. The blue line represents real data taken from the cavity, while the green line represents data produced with the simulation used. The main resonant modes will logically be excited by the piezoelectric actuator movement when performing control.

the CNRS simulation. The feasibility of executing the OACS in available hardware platforms within the specified time constraints will be determined.

- » *Lorentz forces detuning.* High variations of the RF field inside the cavity will induce forces in the cavity walls that will slightly deform them. However small, these deformations will cause significant variations in the cavity detuning.
- » *Microphonic perturbations.* Microphonic perturbations are produced by environmental noise and vibrations that may cause drifts from the optimal cavity detuning and excite vibrating mechanical modes.
- » *Uncertainty in the cavity's operation.* The time-varying environment (microphonics, Lorentz forces, and beam intensity) will not only tend to deviate the cavity's critical variables from their SPs but also change the dynamics or cause-effect relationship of the cavity's processes.
- » *Pure time delay.* This delay may be considered a minor control challenge when compared to the previously discussed delays. However, it is relevant to note that there exists a pure time delay (≈ 1 ms) between the control actions applied to the piezoelectric actuator and the beginning of the dynamic response of the cavity resonance frequency. This pure time delay corresponds to one-fifth of the entire dynamic time response and is caused by the piezo's movement transmission across the mechanical system and by the cause-effect dynamics from the mechanical action on the cavity to the electromagnetic wave variation. This kind of time delay can affect the performance of analog control systems, although digital formulations, such as those presented in this article, can help overcome this problem.

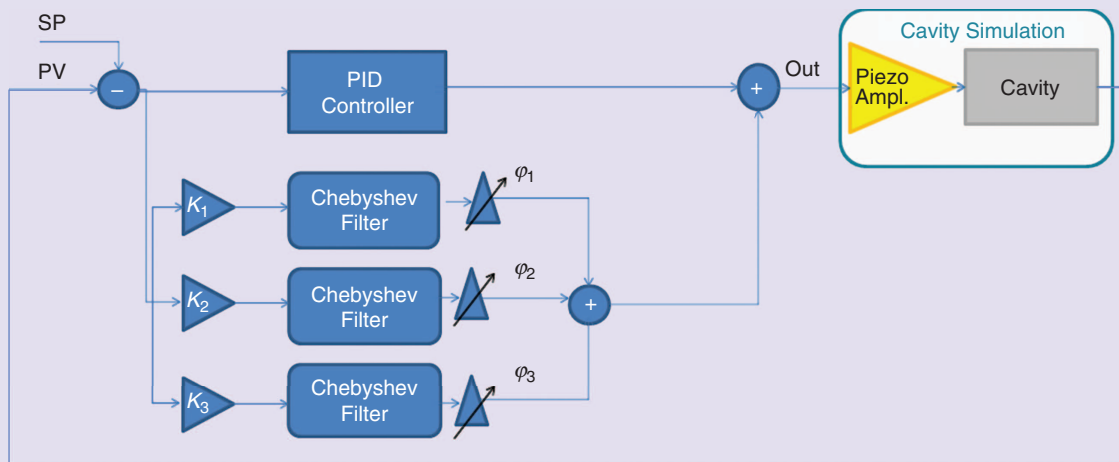


FIGURE 10 Microphonic compensation by Chebyshev filters. This approach combines a proportional-integral-derivative (PID) controller for driving the process variable (PV) to its setpoint (SP), with bandpass Chebyshev type II filters to compensate for microphonic perturbations. Several filters can work in parallel with the PID controller being fed by the error signal, computed as the difference between the PV, which is the cavity's resonant frequency, and its SP. Gains K_i and phase shifts ϕ_i , where i is the number of the filter, are placed in series with the filters, as shown. These parameters are considered separately, given the importance of their tuning to the control system's performance. Under this scheme, bandpass filters act as a feedback mechanism that, prior to applying the error signal to the process, isolates the microphonic frequency.

To address the control challenges here considered for the CTS loop, an OACS was developed and tested on a simulation of the 704.4-MHz, elliptical SC cavity shown in Figure 4. The OACS performance was compared with some of the most significant PID controller-based control systems that were previously applied to the CTS loop [14]–[16]. These systems are described in the following section.

PID-BASED CONTROL SYSTEMS FOR THE CTS LOOP

Many control system designs are based on PID control with (possibly ad hoc) enhancements. For example, an adaptive feedforward technique was proposed [10]–[13], in which a reference signal attempts to compensate for periodic perturbations previously recorded in the facility. This reference signal is processed, prior to its application to the cavity, by an inverse adaptive model of the cavity obtained with techniques such as the least mean squares method. The main limitation of this kind of approach [10] is related to the lack of capacity of PID controllers to achieve the desired level of disturbance attenuation, since their controller gains are limited by stability requirements.

Recently, a feedback alternative was proposed using a series of bandpass filters operating in parallel with a PID controller to enhance compensation at determined critical frequencies [14]–[17]. This bandpass filters technique yielded excellent results that are referenced below.

The original implementation of this approach [14] considered Chebyshev type II bandpass filters acting in parallel with a PID controller to compensate for persistent microphonics. Phase shifters were added [15], [16] in series with the filters, enabling the adjustment of filter delay to enhance

microphonic compensation. This last approach is represented in the block diagram of Figure 10.

In the control system in Figure 10, several filters can work in parallel with the PID controller being fed by the error signal, computed as the difference between the process variable (PV), which is the cavity's resonant frequency, and its setpoint (SP). Gains K_i and phase shifts ϕ_i , where i is the number of the filter, are placed in series with the filters. These parameters were considered separately, given the importance of their tuning to the control system's performance. Under this scheme, bandpass filters act as a feedback mechanism that, prior to applying the error signal to the process, isolates the microphonic frequency. These signals, corrected by the filters, can be tuned to maximize microphonics compensation by modifying the phases (ϕ_i) and the gains (K_i).

Fourth-order Chebyshev type II bandpass filters were considered in [15], [16]

$$y(k) = a_1 y(k-1) + a_2 y(k-2) + a_3 y(k-3) + a_4 y(k-4) + b_0 u(k) + b_1 u(k-1) + b_2 u(k-2) + b_3 u(k-3) + b_4 u(k-4), \quad (7)$$

where $u(k)$ is the original signal before filtering sampled at time k , a_i and b_i are the filters coefficients, and $y(k)$ is the signal after filtering.

The coefficients shown in Table 2 define the Chebyshev type II bandpass filter designed for a frequency of 71 Hz with a sampling time of $2 \mu\text{s}$. At this frequency, a microphonic perturbation was implemented in the simulation, and the filter considered here was used to obtain the results presented in the "Simulation Results" section.

Figure 11 shows the classical shape of the step response of a Chebyshev filter, in this case the one determined by the parameters of Table 2. The figure shows a sinusoidal wave of 71 Hz, of which the amplitude depends on the magnitude of this harmonic component on the filtered signal (in this case a step). The computed Bode diagram of this filter is shown in Figure 12. The frequency response in Figure 12 shows the magnitude of attenuation and the phase shift caused by the filter in the harmonic components of the incoming signal, as a function of their frequency. As can be observed in Figure 12 for 71 Hz, there is no attenuation (≈ 0 dB). There is considerable attenuation for the rest of the frequencies. In this manner, Chebyshev filters separate their design frequency from the rest of the signal.

Chebyshev filter performance was described in [14] and is an appropriate tool for the compensation of microphonics that cause sinusoidal drifts at a determined frequency in the cavity's detuning. Nevertheless, these kinds of filters were conceived for microphonic perturbations that occur in a certain scenario, at a certain time, in a particular facility, and with a particular setup. However, the way in which microphonic perturbations alter the cavity detuning will change according to external factors such as the equipment (that is, pumps and motors) in the facility or the transports surrounding it. Thus, the performance of this type of filter, when facing the uncertainties of a continuous operating facility such as MYRRHA, in which operating circumstances will change while filter parameters remain unchanged, may deteriorate.

ADEX OPTIMIZED ADAPTIVE CONTROL SYSTEMS

Due to the time-varying nature of industrial processes, desirable control performance is often difficult to achieve using fixed parameter controllers. Current industrial applications demonstrated that the use of systems-integrating adaptive controllers in the appropriate control strategy can yield optimized control performance [20]–[23]. This kind of system is referred to as an OACS [26]. When ADEX is the

type of adaptive controller used in the optimized control strategy, the corresponding system is referred to as an ADEX OACS or, simply, ADEX system.

The general ADEX methodology and how ADEX controllers define AP or expert control domains of application within the controller operation are described in "ADEX Optimized Adaptive Controllers and Systems." Operator knowledge of the process dynamics are used in the configuration of the ADEX controller to improve the performance, robustness, and stability of the overall control system. The following section describes the specific AP control algorithms used within the central AP domain of the ADEX controller and its experimental performance on the CTS loop.

Adaptive Predictive Control for the CTS Loop

This section describes the operation algorithm in an AP domain of the ADEX controller applied to the CTS regulation loop. The general methodology of AP expert ADEX control is described in "ADEX Optimized Adaptive Controllers and

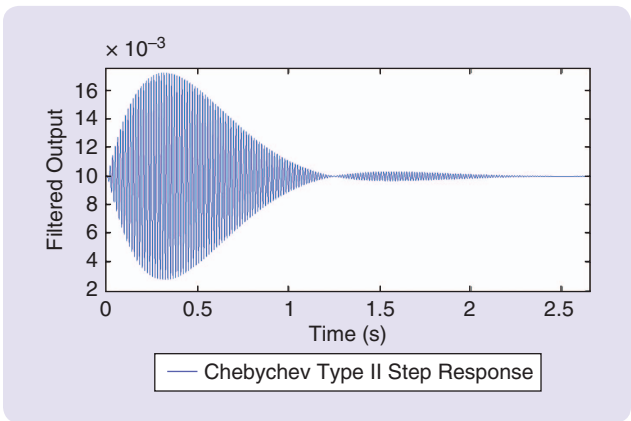


FIGURE 11 A step filtered with a Chebyshev filter designed for 71 Hz. The filtered step response is a sinusoidal wave of 71 Hz, of which the amplitude depends on the magnitude of this harmonic component in the step.

TABLE 2 A Chebyshev type II filter's coefficients for 71-Hz bandpass. These coefficients define the Chebyshev type II bandpass filter designed for a frequency of 71 Hz with a sampling time of 2 μ s. At this frequency, a microphonic perturbation was implemented in the simulation.

Coefficient Chebyshev Type II	Value	Coefficient Chebyshev Type II	Value
a_1	3.98214754	b_0	0.00999999
a_2	-5.96237521	b_1	-0.03984043
a_3	3.97816630	b_2	0.05968248
a_4	-0.99800146	b_3	-0.03984238
		b_4	0.01000097

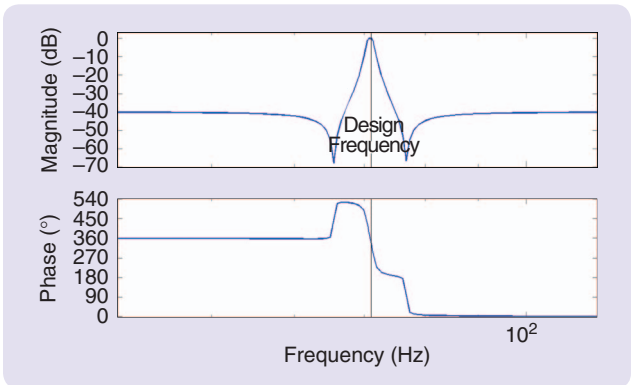


FIGURE 12 A Bode diagram of a Chebyshev type II filter designed for a 71-Hz frequency. The 71-Hz frequency has almost no attenuation (≈ 0 dB), while the rest of the frequencies are considerably attenuated.

ADEX Optimized Adaptive Controllers and Systems

The methodology of the adaptive predictive expert (ADEX) [18], [19] arises from the integration of adaptive predictive control (APC) [24], [25], [53] and expert control [S2], defining domains of operation for each in an integrated structure of control. ADEX methodology enables the controller to be designed in such a way that it detects its current operating domain and uses the best information available from the process to apply APC (AP domain) or expert control (EX domain) accordingly. ADEX control benefits from the experience of the operator and defines the rules governing the use of expert control or the best way of applying APC in each domain of operation. In this way, ADEX overcomes the lack of robustness of APC and can be used to apply optimized control as explained below.

Expert control is applied in operating domains where the basic objective is to lead the process variables (PVs) back toward domains where the application of APC is possible and desirable. APC in these AP domains quickly reduces the prediction error toward zero, which enables the evolution of the PVs to be guided in the desired way, solely restricted by the physical limitations of the process itself. In this way, the criterion for the design of the desired evolution of the PVs does not depend on stability considerations, as in the typical case of control systems based on proportional-integral-derivative controllers, but will be able to focus on optimizing the performance of the process without any restriction other than physical limitations.

AP AND EXPERT DOMAINS OF OPERATION

When an ADEX controller operates in an AP domain, its control algorithms result from the combination of those executing a predictive controller and those executing an adaptive system,

as represented in the block diagram of Figure S3. As shown in Figure S3, the predictive controller and the adaptive system share the same AP model yet execute different functions by assigning equations to the various blocks that describe the operation of a generic AP controller. The dynamics of the generic process considered in Figure S3 can be described by multi-input, multi-output difference equations

$$Y(k) = \sum_{i=1}^h A_i(k) Y(k-i-r) + \sum_{i=1}^f B_i(k) U(k-i-r) + \sum_{i=1}^g C_i(k) W(k-i-r) + \Delta(k), \quad (\text{S17})$$

where $Y(k-i-r)$, $U(k-i-r)$, and $W(k-i-r)$ are, respectively, the increments at time $k-i-r$ of the measured output, input, and measurable disturbance vectors of the process with respect to its steady-state values. $A_i(k)$, $B_i(k)$, and $C_i(k)$ are time-variant matrices of appropriate dimensions that determine the most significant dynamics of the process. $\Delta(k)$ is the perturbation vector, where measurement noises, nonmeasurable perturbations, and other process dynamics are considered, and r represents the pure process time delay.

The AP model used in the adaptive system of Figure S3 calculates an a priori estimation of the process output $\hat{Y}(k)$ as

$$\hat{Y}(k|k-1) = \sum_{i=1}^h \hat{A}_i(k-1) Y(k-i-r) + \sum_{i=1}^f \hat{B}_i(k-1) U(k-i-r) + \sum_{i=1}^g \hat{C}_i(k-1) W(k-i-r). \quad (\text{S18})$$

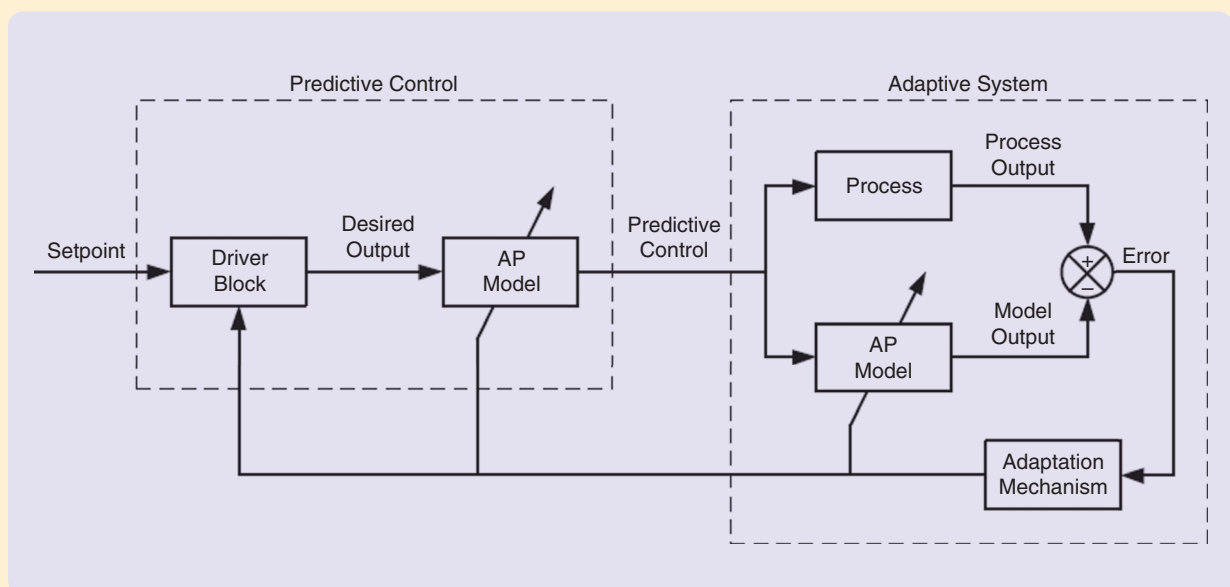


FIGURE S3 A block diagram of adaptive predictive (AP) control.

The adaptation mechanism uses the error of the a priori estimation $Y(k) - \hat{Y}(k|k-1)$ to adjust the AP model parameter matrices \hat{A}_i , \hat{B}_i , and \hat{C}_i at each control time k , to minimize this a priori estimation error or make it to tend toward zero.

The previously considered AP model is used as well to predict, at time k , the process output for time $k+r+1$ as

$$\hat{Y}(k+r+1|k) = \sum_{i=1}^h \hat{A}_i(k) Y(k-i+1) + \sum_{i=1}^f \hat{B}_i(k) U(k-i+1) + \sum_{i=1}^g \hat{C}_i(k) W(k-i+1). \quad (\text{S19})$$

From (S19), the basic strategy of predictive control is to compute the control vector that renders the predicted output $\hat{Y}(k+r+1|k)$ equal to the desired output $Y_d(k+r+1)$ by means of

$$U(k) = \hat{B}_1(k)^{-1} Y_d(k+r+1) - \hat{B}_1(k)^{-1} \left[\sum_{i=1}^h \hat{A}_i(k) \hat{Y}(k-i+1) + \sum_{i=1}^f \hat{B}_i(k) \hat{U}(k-i+1) + \sum_{i=1}^g \hat{C}_i(k) W(k-i+1) \right], \quad (\text{S20})$$

where the desired output $Y_d(k+r+1)$ is computed by the driver block at time k as

$$Y_d(k+r+1) = \sum_{i=1}^t F_i Y(k-i+1) + \sum_{i=1}^s H_i Y_{\text{SP}}(k-i+1), \quad (\text{S21})$$

where $Y_{\text{SP}}(k-i+1)$ represents the value of the setpoint (SP) vector at time $k-i+1$, and matrices F_i and H_i are chosen to account for the desired dynamics.

The previous generic formulation of APC includes an extended strategy for predictive control [46]–[48] in which the desired output $Y_d(k+r+1)$ is the first value of a future process output trajectory that minimizes a performance criterion in a selected prediction horizon λ .

AP controllers are called optimized adaptive controllers [26] when, according to the extended predictive control strategy, the desired value for the previously considered process output is the first one of a future desired process output trajectory that

optimizes a performance criterion in a selected prediction horizon λ . In this case, the predictive control signal is the first one of a corresponding future control sequence that the predictive model forecasts will cause this desired process output trajectory. The envelope of the first values of the different desired output trajectories generated at subsequent control instants k is named desired driving trajectory (DDT) since the values of this trajectory determine the sequence of predictive control values applied to the process.

The diagram in Figure S3 can be simplified to the one shown in Figure S4, which is the diagram generally used to represent the APC methodology. The functional description of the blocks in this diagram can be summarized as follows. *The driver block* generates the DDT that will guide the process output to the SP in an “optimal” way. *The predictive model* calculates the control signal that makes the predicted process output follow the desired trajectory generated by the driver block. *The adaptation mechanism* adjusts the predictive model parameters from the prediction errors to make these errors tend to zero efficiently. Likewise, it informs the driver block of the deviation of the process output with respect to the desired trajectory. In this way, the driver block can redefine the desired trajectory from the actual process output.

The controller configuration for AP domains is done systematically [S3] by setting the values of the structure variables that determine the operation of APC. The most relevant of these structure variables are: 1) the control period; 2) the parameters that determine the AP model structure, including the process time delay; 3) the limits on the input–output variables; 4) the noise level on the process output; 5) the rate of change (RC) of the desired process output trajectory, and 6) the prediction horizon.

When an ADEX controller operates in an expert (EX) domain, it applies rules that imitate the human operator behavior in the same domain of operation. The ADEX controller configuration for EX domains is done systematically, as explained in [S3], by setting the values of tables that determine the rules to be applied for computing the control vector in each specific expert domain.

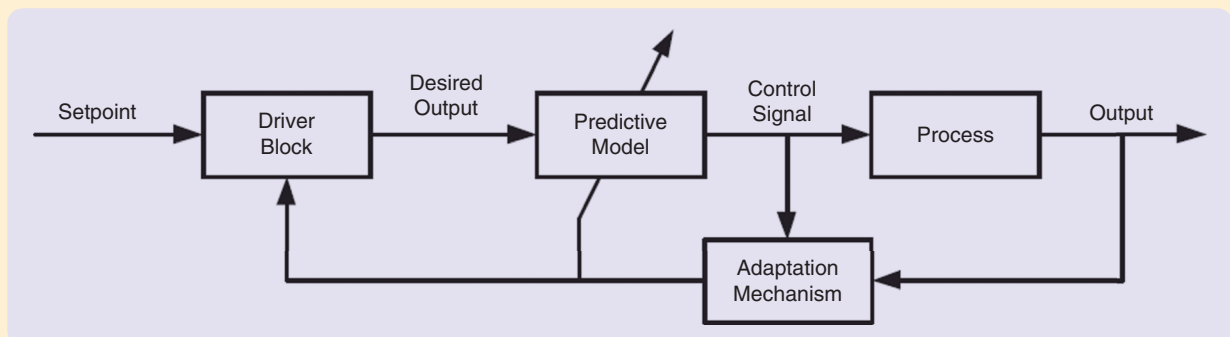


FIGURE S4 A simplified block diagram of adaptive predictive control (APC).

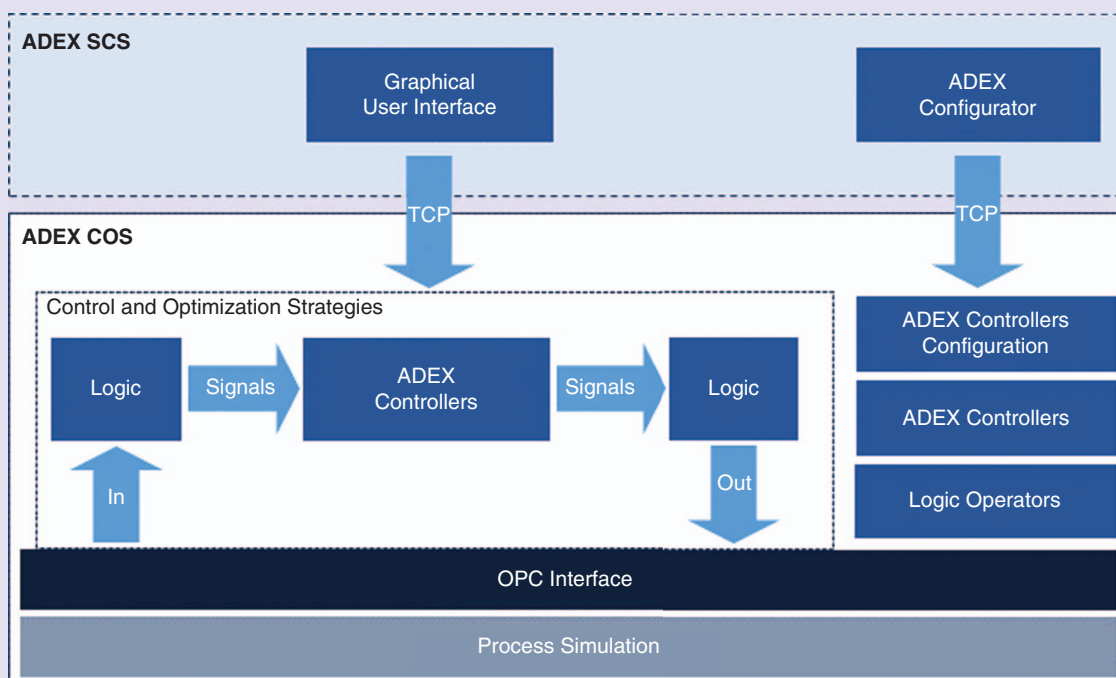


FIGURE S5 The basic structure of adaptive expert control and optimization platform (ADEX COP). This figure represents schematically the implementation of the ADEX COP made of a control and optimization system (COS) and a supervisor and configuration system (SCS). The ADEX COS performs the following steps in every sample time: 1) acquisition of process variables from the process simulator; 2) execution of the control and optimization strategies, including the ADEX controllers; and 3) transfer of the optimized control signals to the process simulator.

ADEX OPTIMIZED ADAPTIVE CONTROL SYSTEMS

The concept of optimized process control performance was introduced in [S4] and described as follows. Optimized process control performance is achieved by a control system able to 1) maintain the PVs under precise control around their SPs with adequately bounded control signals, in spite of changes in process dynamics, context of operation, and noise and perturbations acting on the process; 2) achieve transitions between the attainable operating points in which the PVs are driven through desired trajectories with adequately bounded control signals; and 3) continuously drive the PVs toward their optimal operating points. Obviously, the previous concept of optimized process control performance is not a well-defined mathematical concept. Due to the usual complexity of the in-

dustrial operating context, this concept was derived from an industrial application perspective, where the best possible control performance can only be defined in a qualitative manner and confirmed by the common-sense criteria of the human process operator. Due to the time-varying nature of industrial processes, the desired objective of optimized process control performance is often difficult to attain and maintain using fixed-parameter controllers, such as those derived from control methodologies currently used in industry. Most advanced control solutions are based on fixed-parameter controllers that have limited performance.

It was demonstrated in [S5] that the use of optimized adaptive controllers, integrated in the appropriate control strategy, can approach optimized process control performance in

Systems." This ADEX controller has three different control domains, two expert domains and an AP domain corresponding, respectively, to the upper, lower, and central parts of the range of operation of the cavity frequency detuning. Expert control, using the operator knowledge from the process dynamics, is applied in the expert domains while APC is applied in the AP domain. The block diagram of the APC algorithm applied to the CTS loop is shown in Figure 13.

APC results from the combination of a predictive control scheme with an adaptive system. As shown in the forward path, at each control instant k , a driver block generates a desired process output value (in this case, the desired frequency detuning value) from an SP value (the SP value for the frequency detuning) and the currently measured process output (frequency detuning measurement). A predictive model is then used to compute the

industry. In fact, [S5] included five applications currently optimizing the performance of industrial processes in different domains, such as combined-cycle [20] and coal-fired [S6] power plants (energy), levels in large canals [S7] (water), sulphur recovery plants [S8] in a refinery (petrochemical), and a wastewater treatment plant [S9] (environmental). When a control system, defined by an appropriate control strategy integrating optimized adaptive controllers, is able to achieve optimized process control performance, reference will be made in the sections below to optimized process control strategy and optimized adaptive process control system. When the optimized adaptive controllers are ADEX controllers, reference will be made to ADEX-optimized adaptive control systems, or simply ADEX systems.

IMPLEMENTATION OF ADEX SYSTEMS

The ADEX control and optimization platform (ADEX COP) [S3] used in the implementation of the ADEX system of this project and others is represented in Figure S5. It includes a supervisory and configuration system (SCS) and a control and optimization system (COS). ADEX COP uses LabView as the graphical integrated development environment for the implementation of optimized control strategies. The ADEX SCS allows the development of optimized control strategies (OCSs) for the ADEX COS by means of a graphical user interface that uses ADEX controllers and logic operators stored in the ADEX COS memory. Figure S5 schematically represents the implementation of the ADEX COS, which is described for every control instant in the following steps: 1) acquisition of PVs via OPC from the process simulator, 2) execution of the OCS capable of calculating the optimized control signals, and 3) transfer via OPC of the optimized control signals to the process simulator.

IMPLEMENTATION OF ADEX CONTROLLERS

Figure S6 shows the graphical operator that represents ADEX controllers and is used in the ADEX COP to integrate the ADEX controllers in the optimized control strategy. The ADEX controllers are designed to be multivariable, meaning their inputs or process outputs, SPs, and outputs are vectors. Also, the controller receives the information of the actual input vector applied to the process in the previous control instant, the modes of operation, the controller name, and a signal indicating that

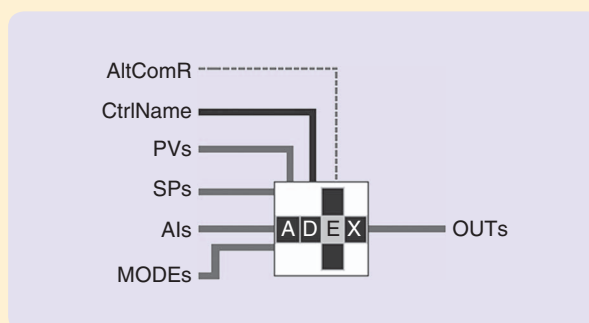


FIGURE S6 An adaptive predictive expert (ADEX) controller graphical operator. The ADEX controllers are designed to be multivariable, which means that their inputs or process outputs (PVs), setpoints (SPs), and outputs (OUTs) are vectors. Also, the controller receives the information of the actual input (AIs) vector applied to the process in the previous control instant, the modes (MODEs) of operation, the controller name (CtrlName), and a signal (AltComR) indicating that the communication with the process simulator is functioning correctly.

the OPC communication with the process simulator is functioning correctly. Likewise, ADEX COP enables the definition and configuration of the EX and AP domains included in a controller.

REFERENCES

- [S2] K. Hiroka, *Industrial Applications of Fuzzy Technology*. New York: Springer-Verlag, 1993.
- [S3] J. M. Martín-Sánchez and J. Rodellar, *Adaptive Predictive Expert Control: Methodology, Design and Application* (in Spanish). UNED, 2005.
- [S4] J. M. Martín-Sánchez, "Editorial: Industrial optimized adaptive control," *Int. J. Adapt. Control Signal Process.*, vol. 26, no. 10, pp. 879–880, 2012.
- [S5] J. M. Martín-Sánchez, "Special issue on industrial optimized adaptive control," *Int. J. Adapt. Control Signal Process.*, vol. 26, no. 10, pp. 879–989, 2012.
- [S6] R. Requena and A. Geddes, "Adaptive predictive expert control of superheated steam temperature in a coal-fired power plant," *Int. J. Adapt. Control Signal Process.*, vol. 26, no. 10, pp. 932–944, 2012.
- [S7] J. V. Aguilar, P. Langarita, L. Linares, J. Rodellar, and J. Soler, "Adaptive predictive expert control of levels in large canals for irrigation water distribution," *Int. J. Adapt. Control Signal Process.*, vol. 26, no. 10, pp. 945–960, 2012.
- [S8] A. Raimondi, A. Favela, R. Estrada, A. Nevado, and E. Gracia, "Adaptive predictive control of the sulfur recovery process at PEMEX Cadereyta refinery," *Int. J. Adapt. Control Signal Process.*, vol. 26, no. 10, pp. 961–975, 2012.
- [S9] G. Kandare, D. Viúdez-Moreiras, and F. Hernández-del-Olmo, "Adaptive control of the oxidation ditch reactors in a waste water treatment plant," *Int. J. Adapt. Control Signal Process.*, vol. 26, no. 10, pp. 976–989, 2012.

control signal applied to the process (voltage applied to the piezoelectric actuator), according to the predictive control principle [24] that makes the predicted process output equal to the desired process output. This voltage signal makes the predicted frequency detuning equal to the desired frequency detuning computed by the driver block.

An adaptation mechanism in the feedback path updates the parameters and variables of the driver block and predictive

model. This adaptive (self-tuning) mechanism makes the prediction error on the process output tend toward zero and ensures stability and optimized performance of APC.

AP controllers are called optimized adaptive controllers [26] when, according to the extended predictive control strategy [46]–[48], the desired value for the previously considered process output is the first element of a future desired process output trajectory that optimizes a performance criterion in a

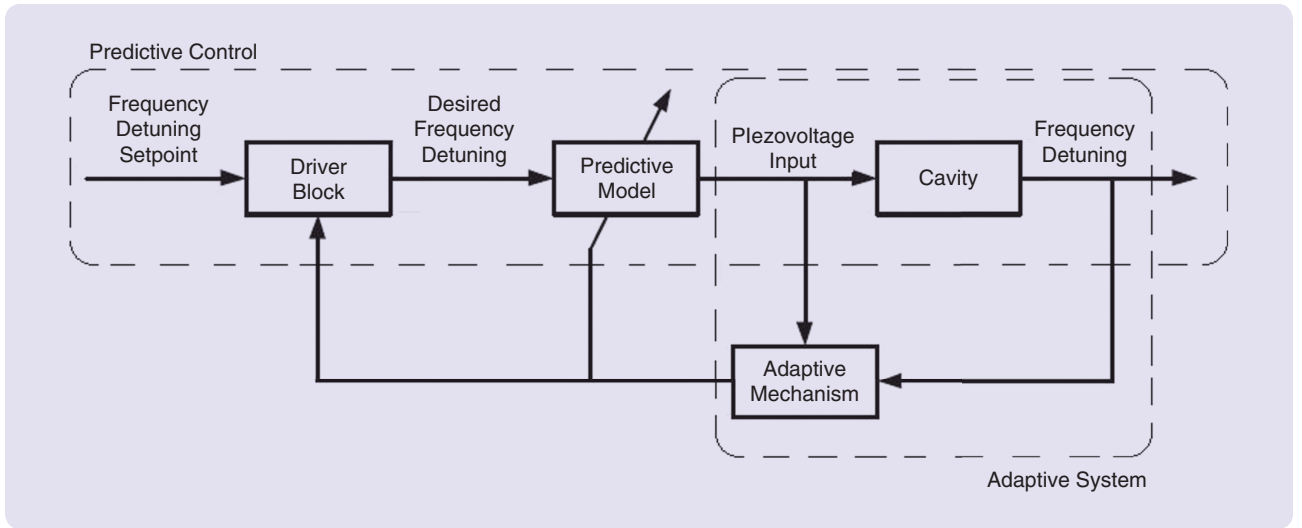


FIGURE 13 Adaptive predictive control for the cold tuning system loop. The driver block on the upper-left part of the figure generates the desired frequency detuning value at each control instant k from the frequency detuning setpoint and the frequency detuning measurement. The predictive model then computes the voltage applied to the piezoelectric actuator to make the predicted frequency detuning equal to the desired frequency detuning computed by the driver block. Finally, an adaptive mechanism uses the piezovoltage applied to the cavity and the frequency detuning values to update the predictive model parameters, to make the prediction error tend toward zero.

selected prediction horizon λ . In this case, the predictive control signal is the first element of a corresponding future control sequence that the predictive model predicts will cause the desired process output trajectory. The APC algorithm was applied to the CTS loop with a control period of 2 ms, using the extended strategy of predictive control, as described below.

To generate the desired process trajectory for the frequency detuning, at each control time k , the driver block uses a specific case of the generic AP model (S19) described in “ADEX Optimized Adaptive Controllers and Systems,” customized for the CTS loop. Since the time delay in the CTS (1 ms) is shorter than the control period, the AP model does not consider any pure time delay, and the prediction at time $k+1$ of the process output made by the CTS AP model is

$$\hat{y}(k+1|k) = \hat{a}_1(k)y(k) + \hat{a}_2(k)y(k-1) + \hat{b}_1(k)u(k) + \hat{b}_2(k)u(k-1) + \hat{b}_3(k)u(k-2), \quad (8)$$

where $\hat{a}_1(k)$, $\hat{a}_2(k)$, $\hat{b}_1(k)$, $\hat{b}_2(k)$, and $\hat{b}_3(k)$ are the AP model parameters as updated by the adaptation mechanism at time k ; $y(k)$ and $y(k-1)$ are the values of the frequency detuning at times k and $k-1$; and $u(k)$, $u(k-1)$, and $u(k-2)$ represent the voltage values applied to the piezoelectric at times k , $k-1$, and $k-2$, respectively. Two parameters $\hat{a}_i(k)$ and three $\hat{b}_i(k)$ were chosen empirically to define the structure of the AP model for this application after trying different AP model configurations in the control simulation.

The recursive prediction of future process output values $\hat{y}(k+j|k)_{(j=1,\dots,\lambda)}$ in the prediction horizon $[k+1, k+\lambda]$ is

$$\begin{aligned} \hat{y}(k+j|k) = & \hat{a}_1(k)\hat{y}(k+j-1|k) + \hat{a}_2(k)\hat{y}(k+j-2|k) \\ & + \hat{b}_1(k)\hat{u}(k+j-1|k) + \hat{b}_2(k)\hat{u}(k+j-2|k) \\ & + \hat{b}_3(k)\hat{u}(k+j-3|k), \quad \text{for all } j = 1, \dots, \lambda, \end{aligned} \quad (9)$$

where $\hat{u}(k+j|k)_{(j=0,\dots,\lambda-1)}$ represents the corresponding process input sequence and

$$\begin{aligned} \hat{y}(k+1-i|k) &= y(k+1-i), \quad \text{for } i = 1, 2, \\ \hat{u}(k+1-i|k) &= u(k+1-i), \quad \text{for } i = 1, 2, 3. \end{aligned} \quad (10)$$

The driver block, under its general formulation [46], selects at each time k a desired output trajectory y_d , and a predicted process output sequence in the prediction horizon $[k+1, k+\lambda]$, which is caused by a predicted process input sequence in the interval $[k, k+\lambda-1]$, in such a way that both sequences satisfy a certain performance criterion. A performance criterion generally used in practical applications [25] was chosen for this implementation. See conditions 1 and 2.

Condition 1

$\hat{y}_d(k+j|k)_{(j=1,\dots,\lambda)} = \hat{y}(k+j|k)_{(j=1,\dots,\lambda)}$, where

- $\hat{y}_d(k+\lambda|k)$ is the value of the desired output trajectory at time $k+\lambda$. This value is computed at time k as the output value at time $k+\lambda$ of a model reference with a chosen desired dynamics, the same SP input as the driver block, and the same initial values as the predicted output sequence.
- $\hat{y}(k+j|k)$ is the process output sequence predicted by the AP model at time k from the values of the process input sequence $\hat{u}(k+j-1|k)_{(j=0,\dots,\lambda-1)}$.

Current industrial applications demonstrated that the use of systems-integrating adaptive controllers in the appropriate control strategy can yield optimized control performance.

Condition 2

The process input sequence $\hat{u}(k+j-1|k)_{(j=0,\dots,\lambda-1)}$ is constant in the interval of prediction $[k, k+\lambda-1]$, that is, $\hat{u}(k|k) = \hat{u}(k+j-1|k)_{(j=0,\dots,\lambda-1)}$.

The dynamic of the model reference considered in Condition 1 was chosen for this application of second order with a gain of one, a damping ratio of one, and a time constant of 1.5 control periods. Parameter λ defining the prediction horizon was chosen equal to ten control periods.

Under Condition 2, the prediction at time k of the process output at time $k+\lambda$, $\hat{y}(k+\lambda|k)$, obtained by the AP model (9), can be computed as

$$\hat{y}(k+\lambda|k) = \hat{a}_{1\lambda}(k)y(k) + \hat{a}_{2\lambda}(k)y(k-1) + \hat{b}_{1\lambda}(k)\hat{u}(k|k) + \hat{b}_{2\lambda}(k)u(k-1) + \hat{b}_{3\lambda}(k)u(k-2), \quad (11)$$

where the parameters $\hat{a}_{1\lambda}(k)$, $\hat{a}_{2\lambda}(k)$, $\hat{b}_{1\lambda}(k)$, $\hat{b}_{2\lambda}(k)$, and $\hat{b}_{3\lambda}(k)$ are obtained by recursive algorithms from the AP model parameters in (8), $\hat{a}_1(k)$, $\hat{a}_2(k)$, $\hat{b}_1(k)$, $\hat{b}_2(k)$, and $\hat{b}_3(k)$, as shown in [49]. Equation (11) can be written as

$$\hat{y}(k+\lambda|k) = \hat{\theta}_{0\lambda}(k)^T \phi(k) + \hat{\theta}_{1\lambda}(k)\hat{u}(k|k), \quad (12)$$

where

$$\begin{aligned} \hat{\theta}_{0\lambda}(k)^T &= [\hat{a}_{1\lambda}(k), \hat{a}_{2\lambda}(k), \hat{b}_{2\lambda}(k), \hat{b}_{3\lambda}(k)], \\ \hat{\theta}_{1\lambda}(k) &= \hat{b}_{1\lambda}(k), \end{aligned} \quad (13)$$

$$\phi(k)^T = [y(k), y(k-1), u(k-1), u(k-2)]. \quad (14)$$

Taking into account Condition 1 and using (12), the control signal $u(k)$ is computed

$$u(k) = \hat{u}(k|k) = \hat{\theta}_{1\lambda}(k)^{-1} [y_d(k+\lambda|k) - \hat{\theta}_{0\lambda}(k)^T \phi(k)]. \quad (15)$$

In the implementation performed for the CTS loop, the sequence of operations required to implement (15) is executed under the incremental approach described in [50].

To estimate the process output, at each control time k , the AP model uses a particular case of the generic AP model described by (S18), presented in “ADEX Optimized Adaptive Controllers and Systems,” and customized for the CTS loop. Thus, the a priori process output estimation $\hat{y}(k|k-1)$ made by the CTS AP model is

$$\begin{aligned} \hat{y}(k|k-1) &= \hat{a}_1(k-1)y(k-1) + \hat{a}_2(k-1)y(k-2) + \hat{b}_1(k-1) \\ &\times u(k-1) + \hat{b}_2(k-1)u(k-2) + \hat{b}_3(k-1)u(k-3), \end{aligned} \quad (16)$$

and the error of this estimation is

$$e(k) = y(k) - \hat{y}(k|k-1). \quad (17)$$

The adaptive algorithms used in the adaptation mechanism of the present implementation are similar to those considered in [50] but include a criterion for stopping parameter adaptation of the type used in [51] and [52]. Thus, the estimated error drives the computation of the parameters $\hat{a}_i(k)$ and $\hat{b}_i(k)$ by gradient parameter algorithms

$$\begin{aligned} \hat{a}_i(k) &= \beta_{ai}\alpha(k)e(k)y(k-i) + \hat{a}_i(k-1), \quad \text{for } i = 1, 2, \\ \hat{b}_i(k) &= \beta_{bi}\alpha(k)e(k)u(k-i) + \hat{b}_i(k-1), \quad \text{for } i = 1, 2, 3, \end{aligned} \quad (18)$$

where

$$\alpha(k) = \left(1 + \sum_{i=1}^2 \beta_{ai}y(k-i)^2 + \sum_{i=1}^3 \beta_{bi}u(k-i)^2 \right)^{-1}, \quad (19)$$

and the values of the coefficients β_{ai} and β_{bi} are conveniently chosen [50] when adaptation takes place but become equal to zero, at any time k , when a criterion to stop parameter adaptation is fulfilled. This criterion complies with the stability requirements for the adaptive predictive controller in an industrial context, ensuring that the norm of the parameter's error vector (that is, the difference between a vector formed by the process parameters and a vector formed by the AP model parameters) is always reduced when parameter adaptation occurs [19].

Experimental Interpretation of APC Operation in the CTS Loop

In this section, an illustrative example of the APC algorithm described in the previous section is applied to a CTS loop simulation without microphonics. The simulation scenario considers a field increase inside the cavity, which will be a frequent procedure when the accelerator is in service. The main variables of the cavity and the AP algorithm operation are depicted in Figure 14. The variables of the trend curves in the components of Figure 14 are as follows. The green line in Figure 14(a) is the evolution of the field inside the cavity. The blue and red lines in Figure 14(b) represent the cavity frequency detuning and its SP values, respectively. The blue line in Figure 14(c) shows the voltage

applied by APC to the piezoelectric actuator. The blue and red lines in Figure 14(d) display the prediction error computed as in (17) and the zero value, respectively. The blue and green lines in Figure 14(e) detail the evolution of the $\hat{a}_1(k)$ and $\hat{a}_2(k)$ AP model parameters, respectively. The blue, green, and yellow lines in Figure 14(f) represent the evolution of the $\hat{b}_1(k)$, $\hat{b}_2(k)$, and $\hat{b}_3(k)$ AP model parameters, respectively.

After 20 ms from the start of the simulation, the field starts to increase [Figure 14(a)], and 40 ms later it stops increasing. It starts to increase again around 70 ms and stops around 90 ms. Note that when the field slope changes, Lorentz forces deviate the frequency detuning from its SP [Figure 14(a)]. These forces act as unknown perturbation, of which the dynamics are not considered in the AP model. The forces have two effects; the first is deviating the frequency detuning under control, and the second is changing the process dynamics (that is, changing the dynamic relationship between voltage applied to the piezoelectric and frequency detuning). Each time that the frequency

detuning is deviated from the SP by the Lorentz forces, the absolute value of the prediction error increases [Figure 14(d)]. The adaptation mechanism, driven by this error, adjusts the AP model parameters [Figure 14(e) and (f)]. The prediction error returns toward zero as the frequency detuning stabilizes for a short time, until the new field slope changes, again producing new Lorentz forces. Along with the adaptation mechanism operation, predictive control is applied on the piezoelectric voltage [Figure 14(c)] and stabilizes the frequency detuning close to its SP when the prediction error comes back to zero and the AP model parameters stabilize their values. This situation is an indication that the new process dynamics has been identified with a view to control by the AP model parameters. This kind of identification was considered in [25] and [53].

As an illustrative example of APC performance, when a process dynamic change is produced, the error will increase and the adaptation mechanism will identify the change in dynamics, making the error return toward zero. At the same time, the predictive control signal compensates the

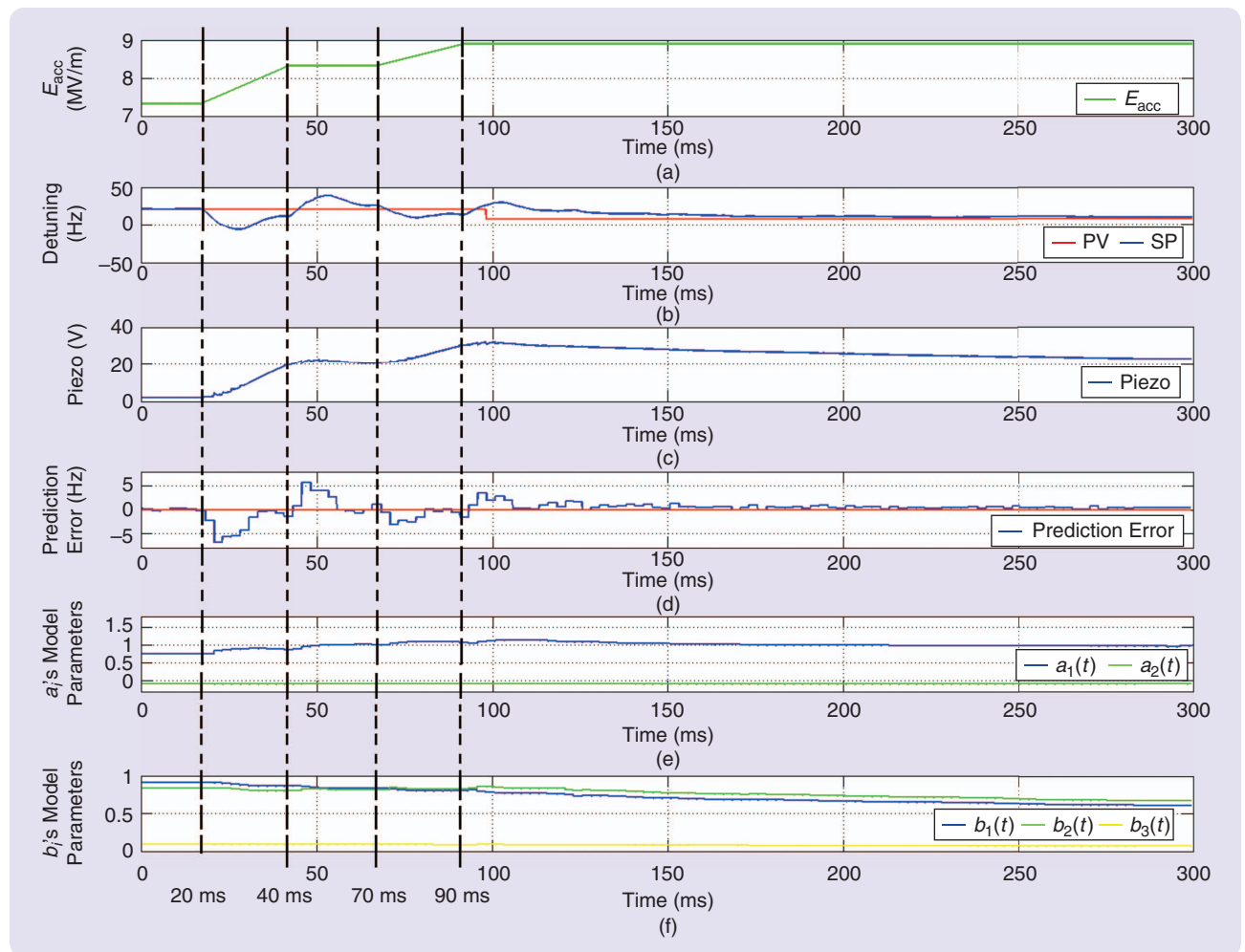


FIGURE 14 An adaptive predictive control (APC) application to the simulated cavity operation. The (a) field inside the cavity, (b) cavity frequency detuning and its setpoint (SP), (c) voltage applied to the piezoelectric actuator, (d) APC prediction error, (e) AP model $\hat{a}_i(k)$ parameters, and (f) AP model $\hat{b}_i(k)$ parameters. PV: process variable.

effect of the perturbation that created the process dynamic change, driving the PV under control toward its SP.

DESIGN OF THE OPTIMIZED CONTROL STRATEGY

The control strategy for the CTS loop was designed to address the main control challenges, described previously. The bases for addressing these challenges are explained as follows.

- » *Dynamics of the cavity resonance frequency:* The main control challenge that represents the dynamic complexity of the CTS loop was addressed by integrating an ADEX controller and filtering tools in the control strategy. The filtering tools will avoid the excitation of inherent and externally induced mechanical resonant modes, whereas the ADEX controller will address the dynamic complexity of the cavity.
- » *Time constraints:* The ADEX controller yielded satisfactory performance in the high-fidelity simulation of the CTS loop with a control period of 2 ms, which makes the required execution time compatible with any adequate processing hardware.
- » *Lorentz forces detuning:* Detuning is determined by the field inside the cavity that is measurable. The effect was anticipated in the control strategy, by the design of a Lorentz anticipation block, which is described below.
- » *Microphonics perturbations:* Prior filtering compensation techniques with excellent results [14], [15] were used by the optimized control strategy.
- » *Uncertainty in the cavity's operation:* The time-varying environment (microphonics, Lorentz forces, and beam intensity) will not only tend to deviate the cavity's critical variables from its SPs but also change cavity dynamics. The ADEX adaptation mechanism can track the cavity dynamics, avoiding deterioration experienced by fixed-parameter control systems and optimizing the CTS loop control performance.
- » *Pure time delay.* The time delay of approximately 1 ms in the CTS is approximately half of the chosen control period. Therefore, there will be no pure time delay in the AP model difference equation (9) that, with said control period, describes the process dynamics. However, the value of parameter $b_1(k)$ and, consequently, the rest of the parameters of the AP model, will be influenced by the time delay. The adaptive predictive feature of the ADEX controller will identify the effect of the time delay on the process model parameters and will account for it in the computation of the control action.

The optimized control strategy used for the CTS loop is described in detail below.

Means to Avoid Exciting Resonant Modes: Notch Filters

Notch filters belong to the family of the infinite impulse response filters. A notch filter is a band-reject filter. This

means that any signal that is filtered by a notch filter designed for a certain frequency will attenuate its harmonic components at that frequency.

For the implementation of the optimized control strategy, second-order filters were considered. The behavior of this filter is determined by

$$y(k) = a_1y(k-1) + a_2y(k-2) + b_0u(k) + b_1u(k-1) + b_2u(k-2), \quad (20)$$

where $u(k)$ is the input value to the filter at the sampling time k , and $y(k)$ is the output or filtered signal value at the same sampling time k . In addition, a_1 , a_2 , b_0 , b_1 , and b_2 are the filter coefficients that must be correctly adjusted to eliminate the desired frequency for the input signal u . The coefficients in Table 3 define a notch filter designed to eliminate an 80-Hz frequency, considering a sampling time of 0.2 ms.

The frequency response of Figure 15 shows the magnitude attenuation and the phase shift caused by the filter, as a function of the frequency of the incoming signal. It can be observed that the maximum attenuation occurs at 80 Hz. It can also be observed that notch filters not only reject the frequency they have been designed for but also attenuate

TABLE 3 Notch filter coefficients for 80-Hz band reject, defined for 0.2-ms sampling time.

Notch Coefficient	Value	Notch Coefficient	Value
a_1	1.85929	b_0	1
a_2	-0.868712	b_1	-1.98849
		b_2	0.997907

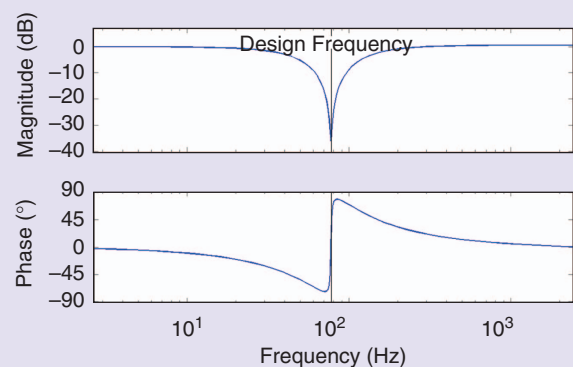


FIGURE 15 A Bode diagram of a notch filter designed for 80-Hz frequency. The filter attenuates the design frequency and frequencies surrounding it. Although the width of the attenuation band can be modified through filter design, a wide band could be helpful in case the resonant frequency to be suppressed does not exactly match the design frequency of the filter.

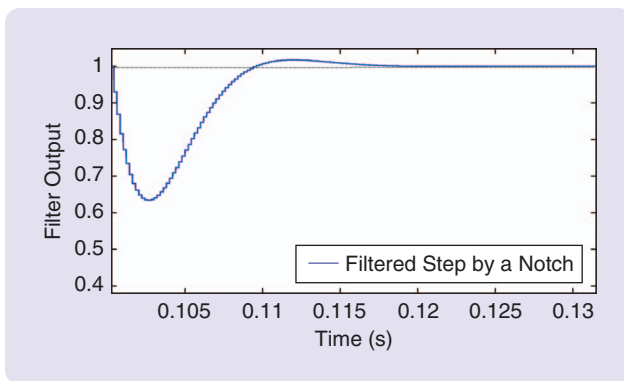


FIGURE 16 A step filtered with a notch filter designed for 80 Hz.

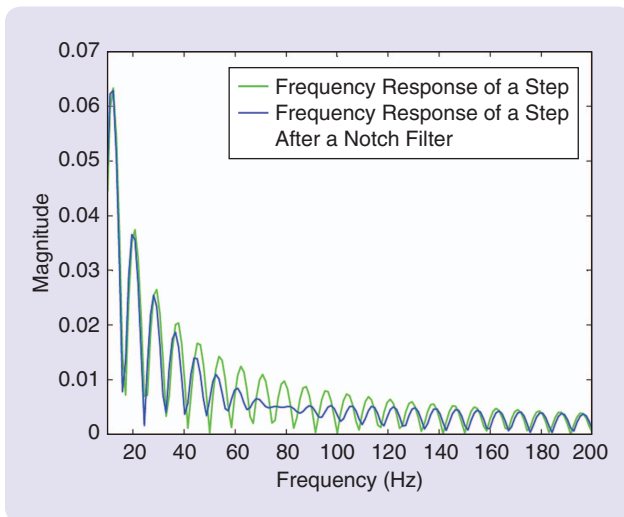


FIGURE 17 Fast Fourier transforms (FFTs) of a step and a step filtered with a notch designed for 80 Hz. The green line shows the FFT, and the blue line shows the FFT of the step filtered by the notch filter. The figure illustrates how the notch filter has attenuated the harmonic components surrounding 80 Hz present in the unfiltered step signal.

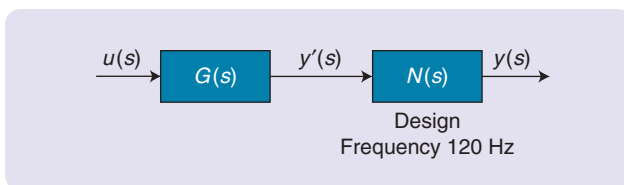


FIGURE 18 Cavity and notch filter transfer functions placed in series. When designed for the frequency of a resonant mode (120 Hz) and placed after the cavity, the notch filter will eliminate the resonant mode effect from its output.

frequencies that are located near the design frequency. Although this side effect can be modified through filter design, certain attenuation at frequencies surrounding the design frequency will not be completely avoided.

Figure 16 shows the classical shape of the step response of a notch filter. In fact, it is the step response corresponding to the filter defined by the coefficients in Table 3. This is

illustrative of the “kickback” produced by the notch filter to avoid the presence of determined harmonic components in the step.

In Figure 17, the fast Fourier transform (FFT) of a step is depicted in green and shows the magnitude of each harmonic component of the step signal. The same figure presents, in blue, the FFT of the step filtered by the notch filter defined by the coefficients of Table 3. The notch filter attenuates the harmonic components around 80 Hz present in the unfiltered step signal.

A notch filter designed for adequate frequency and placed after the cavity should be capable of eliminating some of the resonant modes observed in Figure 9. Figure 18 shows the transfer function of the cavity ($G(s)$), plotted in Figure 9) and the notch transfer function ($N(s)$) placed in series, to eliminate a resonant frequency at 120 Hz.

Figure 19 illustrates the behavior of the cavity with and without filtering. In Figure 19(a), the red line represents the simulated cavity detuning response after a step from 0 to 1 V at a sampling time of 0.1 s. This corresponds to the signal $y'(s)$ detailed in Figure 18 but in the time domain. The red line in Figure 19(b) presents the FFT of this response, which shows the resonant modes that were excited by the step. It must be noted that the main resonant modes correspond to those shown in Figure 9. The simulated cavity detuning ($y'(s)$) processed by the notch filter designed for 120 Hz [whose attenuation in decibels for frequencies up to 250 Hz is shown in Figure 19(c)] is represented in blue in Figure 19(a). This plot shows the filtered cavity detuning that corresponds to $y(s)$ but in the time domain. The FFT of the filtered cavity detuning is represented in blue in Figure 19(b). Comparing both the detuning FFT and the filtered detuning FFT in Figure 19(b), it is determined that the notch filter has attenuated the resonant modes that were near 120 Hz.

The cavity detuning response and its FFT, detailed in red in Figure 19(a) and (b), respectively, have shown how the resonant modes of the simulated cavity were excited by a step input signal with the setup considered in Figure 18. However, if the notch filter is placed before the cavity, as shown in Figure 20, the $y(s)$ response to one step in the input signal $u(s)$ will be the same as that obtained by the setup in Figure 18. This is represented by the blue line in Figure 19(b). This is because the transfer functions of the entire system shown in Figures 18 and 20 are identical due to the commutative property.

The setup of Figure 20 has the advantage that the content in the resonance frequency rejected by the notch filter was previously attenuated by the filter in the input signal to the simulated cavity. Hence, the input signal to the cavity will have an attenuated effect on the excitation of the resonance frequency. The setup shown in Figure 20 is to be considered within the optimized control strategy for the use of notch filters to avoid the excitation of resonance frequencies of the cavity by the controller actions.

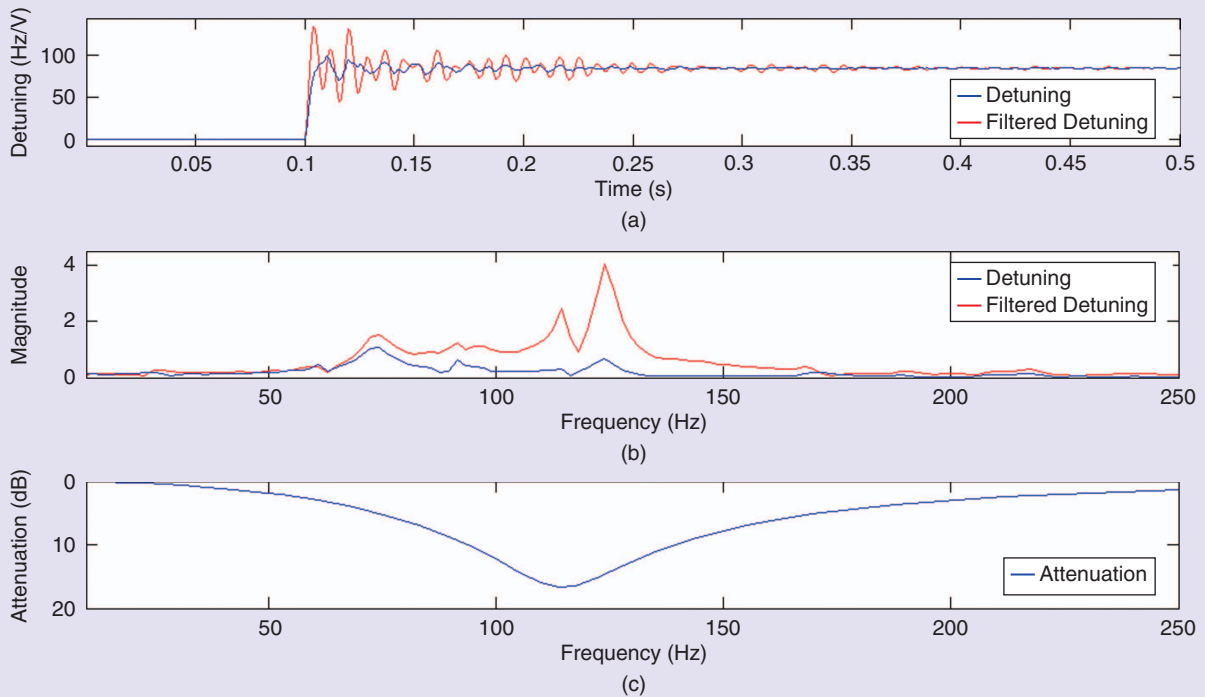


FIGURE 19 Filtered and unfiltered cavity detuning, fast Fourier transforms (FFTs), and filter attenuation. (a) Resonance frequency detuning and filtered detuning time responses to 1-V step in piezo, (b) FFT responses of detuning and filtered detuning after 1-V step in piezo, and (c) filter attenuation in the frequency range.

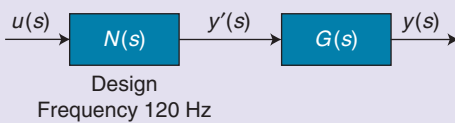


FIGURE 20 The notch filter and cavity transfer functions placed in series. This setup has the advantage that the resonance frequency rejected by the notch filter was previously attenuated in the input signal to the simulated cavity. Hence, the input signal to the cavity will have an attenuated effect on the excitation of the resonance frequency. This distribution is considered within the optimized control strategy to avoid the excitation of resonant modes of the cavity by the controller actions.

Integration of Notch Filters in the Optimized Control Strategy

As analyzed previously, the notch filters avoid exciting the resonant modes of the cavity if they are placed before the piezoelectric actuator (that is, at the output of the controller). In addition to the 120-Hz filter, a notch filter with a wide rejection band was designed at 80 Hz to attenuate the resonant modes found at 73 and 90 Hz that still remain in Figure 19(b). Thus, a preliminary optimized control strategy aimed at avoiding the excitation of the cavity resonance frequencies is shown in Figure 21. Figure 22 compares the step response without notch filtering in red, previously shown in Figure 19, and the

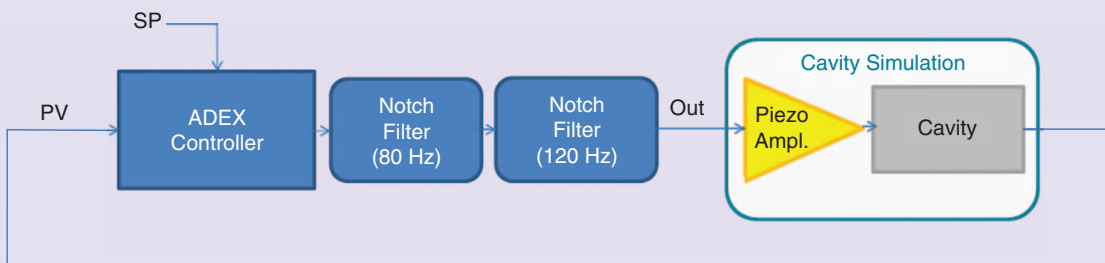


FIGURE 21 A first preliminary control strategy for the cold tuning system loop. Notch filters avoid exciting the resonant modes of the cavity if they are placed before the piezoelectric actuator (that is, at the output of the controller). Two notch filters at 120 and 80 Hz were considered. However, the last one had a wide rejection band to attenuate the simulated cavity's resonant modes at 73 and at 90 Hz. PV: process variable; SP: setpoint.

step response with the notch filters (shown in Figure 21) in blue.

Placing the notch filters after the controller output has certain limitations that must be considered. Imagine a microphonics excitation at 120 Hz on the cavity. The controller would not be able to react against it, since the notch filters would suppress the control action's harmonic component necessary to eliminate this perturbation. Therefore, if this strategy is applied, it is necessary to have an additional strategy not affected by the notch filters that can effectively address this kind of perturbation.

Additionally, since there will be certain frequencies that the controller is unable to handle, due to the notch filters applied to its outputs, the controller should not generate control actions with components trying to compensate for the content in those frequencies in the detuning signal. These kinds of components will have no effect on the frequency contents they intend to correct but may deteriorate the control performance for the rest of the harmonic components of the cavity output variable or detuning. Therefore, it would be advisable to filter the cavity detuning with

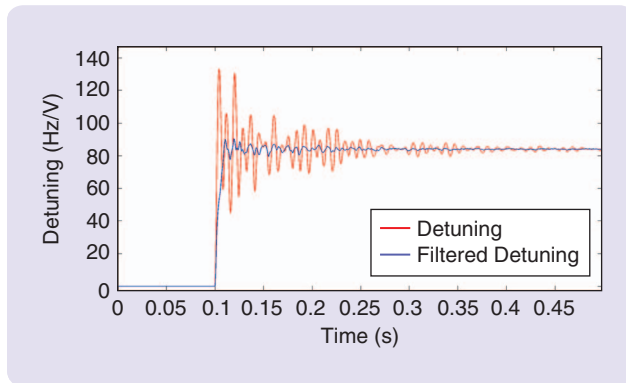


FIGURE 22 A 1-V step response of $N(s) + G(s)$: without (red) and with (blue) notch filters. This figure allows for comparing the step response of the simulated cavity without notch filtering and the step response with the notch filters in blue.

the same notch filters that filter the controller output. This means changing the first preliminary control strategy shown in Figure 21 to the second preliminary control strategy shown in Figure 23.

Integration of Chebyshev Filters in the Optimized Control Strategy

The optimized control strategy integrates Chebyshev filters to attenuate the frequency component of the cavity's resonance frequency detuning that is induced by external perturbations and cannot be compensated by the controller actions when limited by notch filtering. These filters were introduced in [14]–[16] for this application. This kind of control scheme is represented in Figure 24. Three Chebyshev filters were considered for the control of the CNRS cavity simulation, for microphonics corresponding to 1, 71, and 120 Hz.

Feedforward Strategy to Compensate for Lorentz Forces Detuning

An optimized control strategy must be particularly careful with Lorentz forces, especially when the SPs of a cavity must be changed. The RF field ramping will cause strong frequency detuning, due to Lorentz forces that will deeply affect the CTS loop performance. Nevertheless, there exists available and useful knowledge about the initiation and evolution of the perturbation and the effect of Lorentz force detuning. Thus, the CTS control loop receives information from the LLRF control loop, indicating when the RF field starts increasing and its evolution. Recall that the exact detuning caused by Lorentz forces is given by (3) in a stationary regime. Therefore if, for example, an adjacent cavity failure occurs and the RF field's amplitude must change from an SP value E_{acc1} to another SP value E_{acc2} to compensate, it would cause a detuning in the stationary regime Δf_{12} , given by

$$\Delta f_{12} = \Delta f_{11} - \Delta f_{12} = K_L (E_{acc1}^2 - E_{acc2}^2). \quad (21)$$

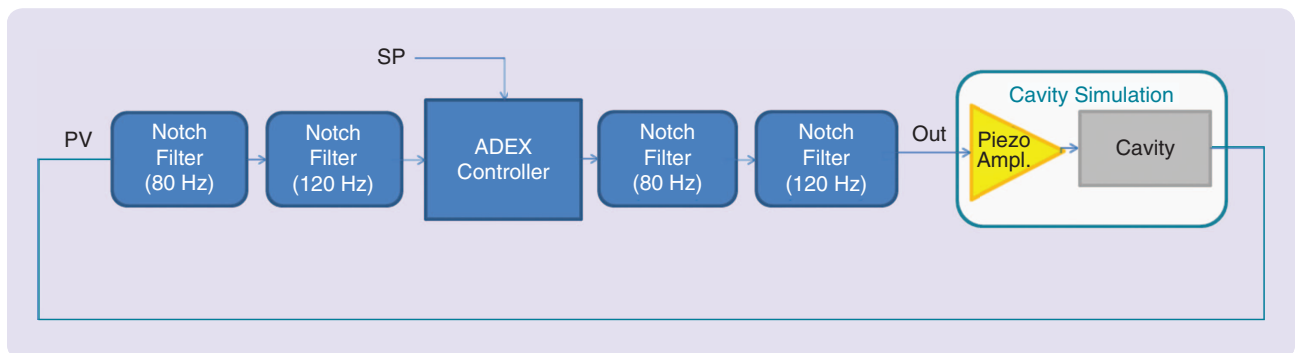


FIGURE 23 A second preliminary control strategy for the cold tuning system loop. Due to the notch filters placed at the controller's output, there will be detuning harmonic components that the controller is unable to correct. Furthermore, the effect of the controller's actions trying to compensate those harmonic components will deteriorate the control performance for the rest of the detuning signal. To avoid this deterioration, the same notch filters placed at the controller's output have been considered at the controller's input. PV: process variable; SP: setpoint.

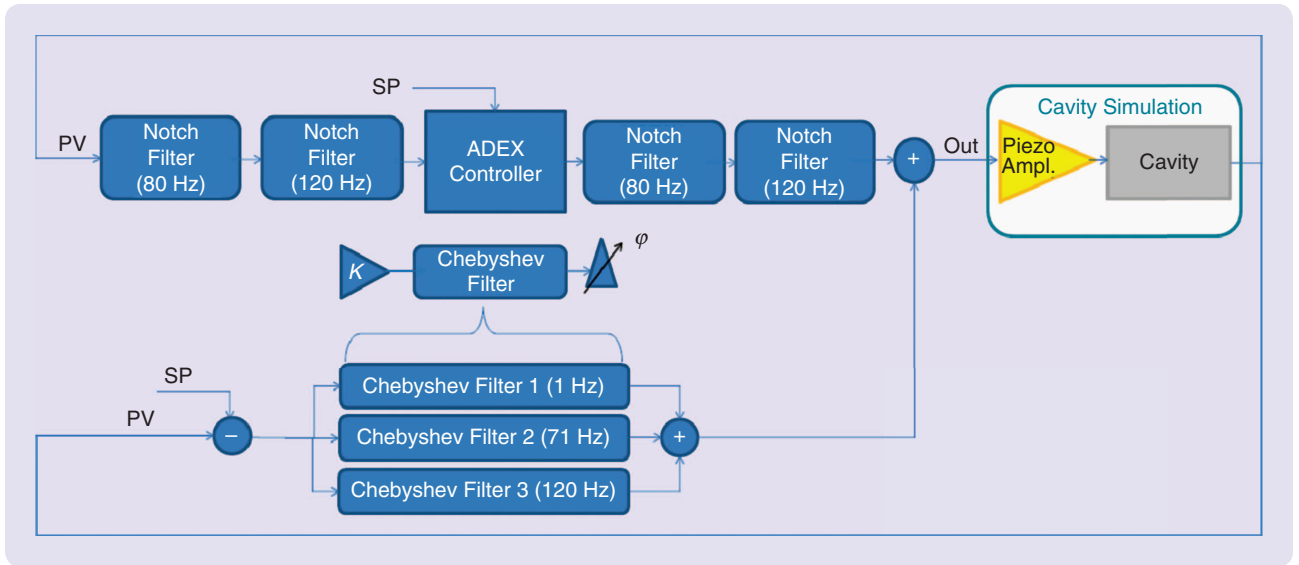


FIGURE 24 A third preliminary control strategy with notch and Chebyshev filters. The control strategy represented in the figure integrates Chebyshev type II filters to attenuate those harmonic components of the cavity's resonance frequency detuning that could be induced by external perturbations and cannot be compensated by the controller actions when limited by notch filtering. Three filters have been considered for the control of the cavity simulation, for microphonics corresponding to 1, 71, and 120 Hz.

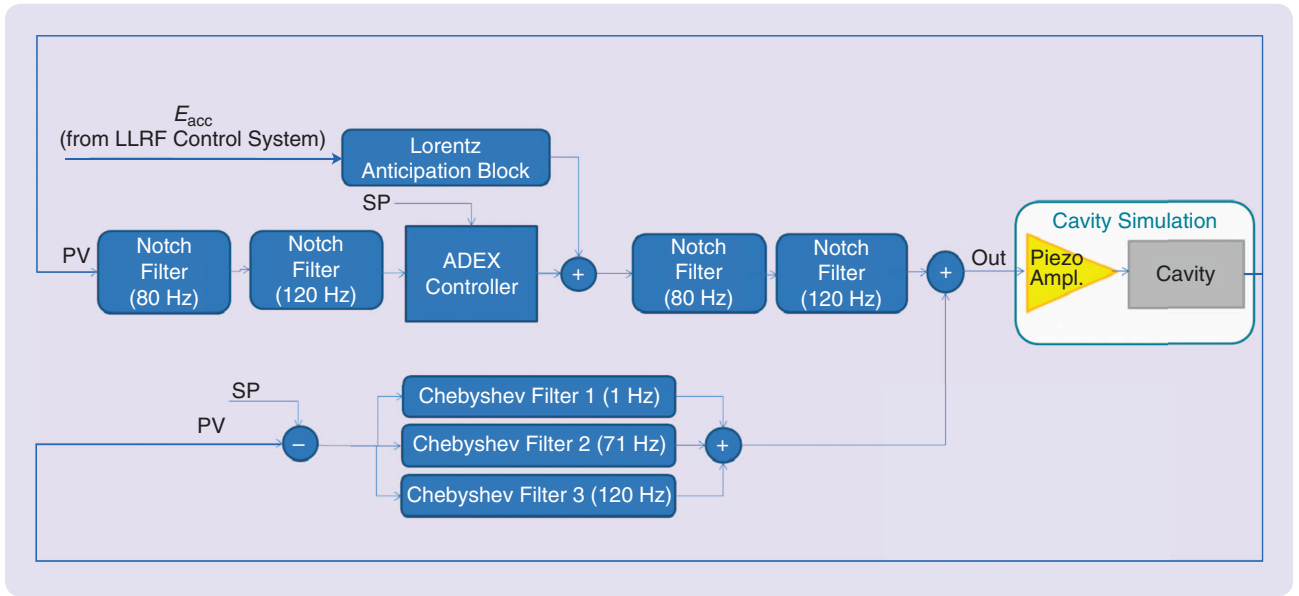


FIGURE 25 The adaptive predictive expert (ADEX) optimized adaptive control system (OACS) design. This block diagram adds to the previous Lorentz anticipation block. The Lorentz anticipation block calculates the necessary ΔV_{12} to compensate for the Lorentz detuning that will be produced by the low-level radio frequency (LLRF) loop, when the radio frequency field's amplitude setpoint (SP) changes. It is observed that the control action produced by the Lorentz anticipation block is summed before the notch filters to avoid the excitation of the resonant modes of the cavity. The block diagram describes the operation of the OACS that has been evaluated in simulation. PV: process variable.

If G is the static gain of the cavity detuning after a change in the piezovoltage, then in the stationary regime, the detuning produced by a voltage variation is

$$\Delta f_{12} = G \Delta V_{12}. \quad (22)$$

Therefore, the convenient change in voltage at the piezo to compensate for the Lorentz forces detuning,

ΔV_{12} , can be calculated from the difference between (21) and (22)

$$\Delta V_{12} = \frac{K_L (E_{acc1}^2 - E_{acc2}^2)}{G} = K (E_{acc1}^2 - E_{acc2}^2), \quad (23)$$

which leaves the control action that should be applied to the piezoelectric actuator as a function of the change in the

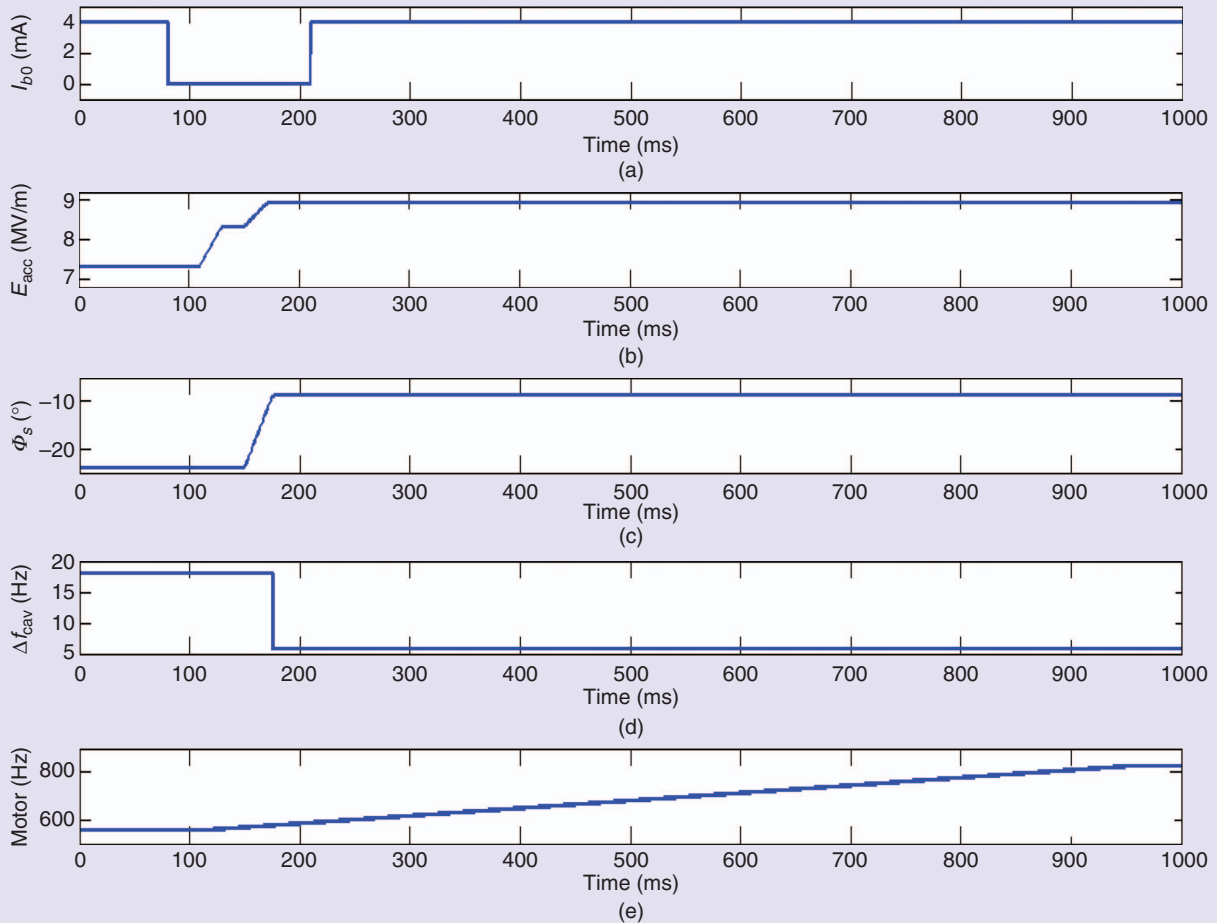


FIGURE 26 A simulation scenario for the retuning procedure of a cavity. (a) The beam intensity throughout the simulation, (b) field setpoint throughout the simulation, (c) phase setpoint throughout the simulation, (d) frequency detuning setpoint throughout the simulation, and (e) detuning caused by the motor's operation throughout the simulation.

field's amplitude ($E_{acc1}^2 - E_{acc2}^2$), since E_{acc1} is the usual operating reference value, E_{acc2} is the RF field's amplitude SP change that can be sent to the CTS control system, and K ($K = K_L / G$) can be calculated empirically. Changes can be anticipated due to Lorentz forces after a cavity failure, by reacting to the RF field's amplitude SP change.

This feedforward strategy modifies the third preliminary optimized control strategy represented in Figure 24 in the manner shown in Figure 25. In Figure 25, the "Lorentz anticipation block" calculates the necessary ΔV_{12} according to (23) to compensate for the Lorentz detuning that will be produced by the LLRF loop when the RF field's amplitude SP changes. It can be noticed that the control action produced by the Lorentz anticipation block is summed before the notch filters to avoid the excitation of the resonant modes of the cavity. The control strategy shown in Figure 25 determines the ADEX system that was applied first to the high-fidelity simulation, anticipating its application to the SC cavity prototype.

The following section presents the results on the control of the CNRS simulated cavity, obtained by three different

control approaches for the CTS control loop: the conventional PID approach, the PID + Chebyshev filters approach previously considered in [14]–[16], and the new OACS approach.

SIMULATION RESULTS

Simulation Software

The ADEX COP platform, described in "ADEX Optimized Adaptive Controllers and Systems," was used to implement the ADEX optimized adaptive control system applied to the superconducting 704.4-MHz elliptical cavity simulator [16]. Between both, an Object Linking and Embedding for Process Control (OPC) [54] communication interface was implemented.

The superconducting 704.4-MHz elliptical cavity simulator was specifically developed to study the cavity's operation, in particular the retuning procedure feasibility [16]. Thus, it is also an efficient tool for developing and testing control algorithms and strategies before their implementation on a real cavity.

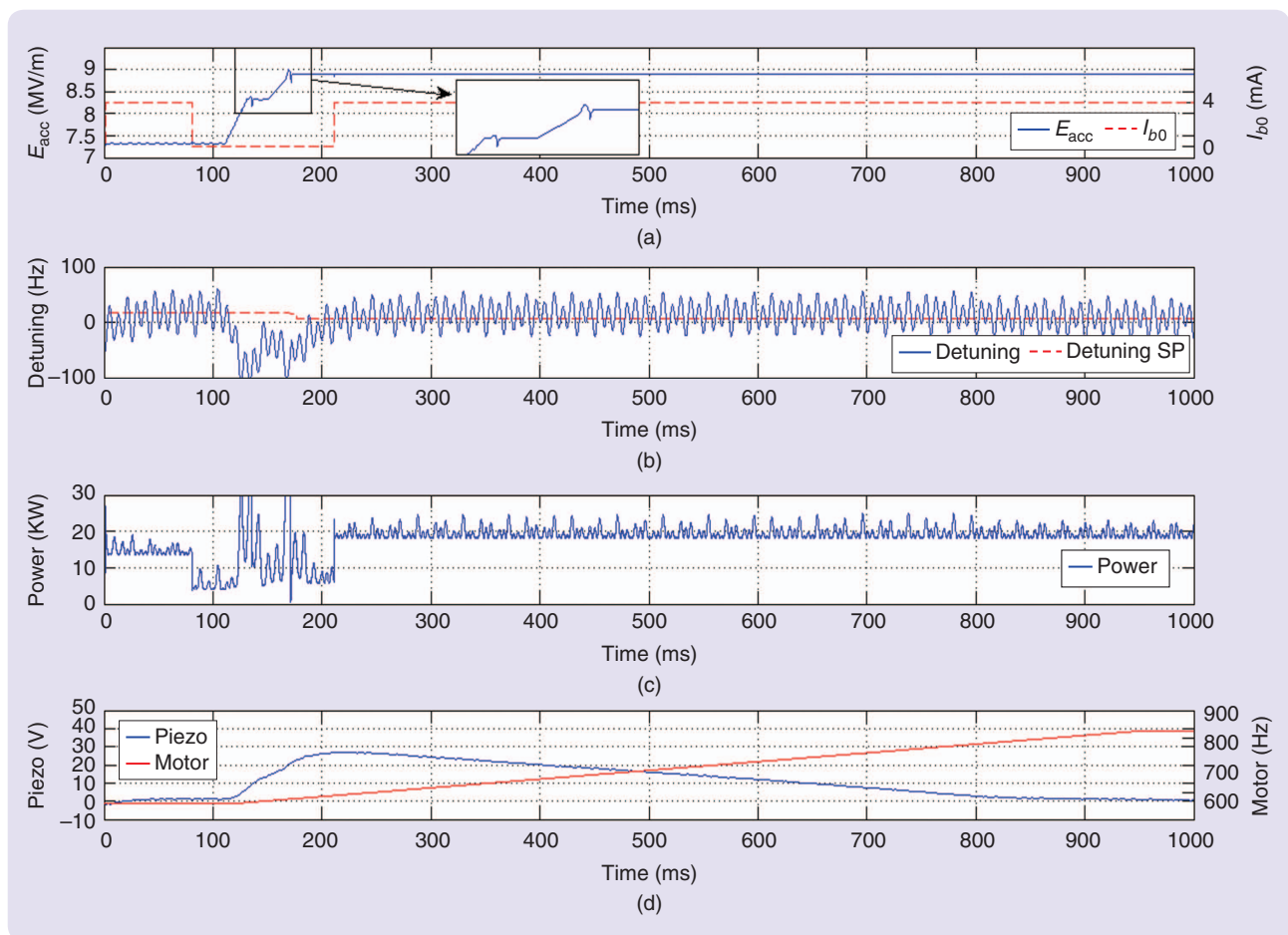


FIGURE 27 A proportional-integral-derivative control approach performance. (a) The amplitude of the field inside the cavity throughout the simulation, (b) the cavity's detuning throughout the simulation, (c) power consumption throughout the simulation, and (d) voltage applied to piezo and motor effect on the cavity detuning.

The simulation reproduces the behavior of the processes involved in the beam acceleration and their associated control loops inside the five-cell elliptical cavity. As the time required by the simulation to compute the processes evolution is greater than the necessary time for the real process evolution to occur, the simulation has been time scaled. The scaling can be fixed by the user within certain limits around the highest simulation speed. Neither vacuum nor cryogenics systems are considered under the scope of the simulation and are considered to work ideally throughout the simulation. LLRF control loops and the CTS control loops are shown in Figure 8.

Both the ADEX COP and the cavity simulator act as OPC clients. Thus, the simulation stores the values of the PVs every second, after performing the necessary computation, on the OPC server. The COP reads these values, executes the control strategy, and writes on the OPC server the pertinent control actions (in this case, only the voltage applied to the piezo). This control action will be read from the OPC server by the simulation and considered for the necessary computation in the next second. This scheme allows the interface to test the control strategy prior to embedding it in

the hardware platform needed to test the system performance in the prototype.

Simulated Scenario

The accelerator operation must be robust against cavity failures. The chosen strategy to recover from a cavity failure is to force the retuning of the adjacent cavities to compensate for the failed one.

To compare the alternative control solutions for the CTS, focus is placed on the cavity scenario that must be retuned to compensate for a failure. This retuning scenario is described on Figure 26. The main steps in the simulations are as follows. At time $t = 80$ ms, the beam is stopped because a failure has been detected in the accelerator. The new SPs for the accelerating fields and phases are sent to the compensation cavity. The beam is resumed 130 ms later, once the accelerating fields and phases have been stabilized on the new targets.

In Figure 26, $t = 0$ ms represents a random moment during the usual accelerator's operation. Figure 26(a) represents the beam intensity (I_{b0}) in the cavity, initially set to 4 mA, which is stopped after the cavity failure and resumed

130 ms later at the initial value. When the beam is stopped, the accelerating field E_{acc} is ramped up into the cavity [Figure 26(b)]. This occurs in two steps to leave time for the CTS loop to compensate for the Lorentz detuning effect caused by the field increase. The phase ϕ_s is also changed to a new SP and ramped to minimize the transient power consumption during the procedure [Figure 26(c)]. Finally, since the cavity SPs have changed, Δf_{cav}^{opt} is also changed according to (S15) presented in “Optimal Frequency Detuning.” At time $t = 180$ ms, the cavity frequency detuning SP is changed to its new optimal value [Figure 26(d)]. Figure 26(e) shows the simulated effect of the motor in the cavity detuning. The motor will slowly compensate for 375 Hz in the cavity detuning, allowing for the faster piezo-compensation to return to its nominal operating range after the transient caused by the SP changes.

Both Lorentz forces and microphonic perturbations have been considered in this scenario. For microphonics, three sinusoidal perturbations were considered, acting at a frequency of 1, 71, and 120 Hz, and provoking maximum deviations of 10, 10, and 20 Hz in the cavity’s frequency detuning.

Simulated Results

PID Approach

The performance of the CTS loop obtained in simulation by a PID controller driving the piezoelectric actuator is illustrated by the experimental results shown in Figure 27. Figure 27 presents the evolution of the accelerating process critical variables in the cavity during 1 s of simulation. The abscissa axis is the time scale in milliseconds. The evolution of the amplitude of the field inside the cavity (E_{acc}) is represented by the blue line in Figure 27(a) along with the beam intensity (I_{b0}), represented by the red dotted line. The evolution of the cavity’s resonance frequency detuning is shown in Figure 27(b) in the blue line while the red line shows its SP. The power consumed to generate the field is shown in Figure 27(c). Finally, the voltage applied to the piezoelectric actuator to drive the cavity’s detuning to its SP is represented by the blue line in Figure 27(d). The simulated motor effect on the cavity detuning is also shown in Figure 27(d) in the red line. The interpretation from the origin of the subsequent steps is as follows. When the beam

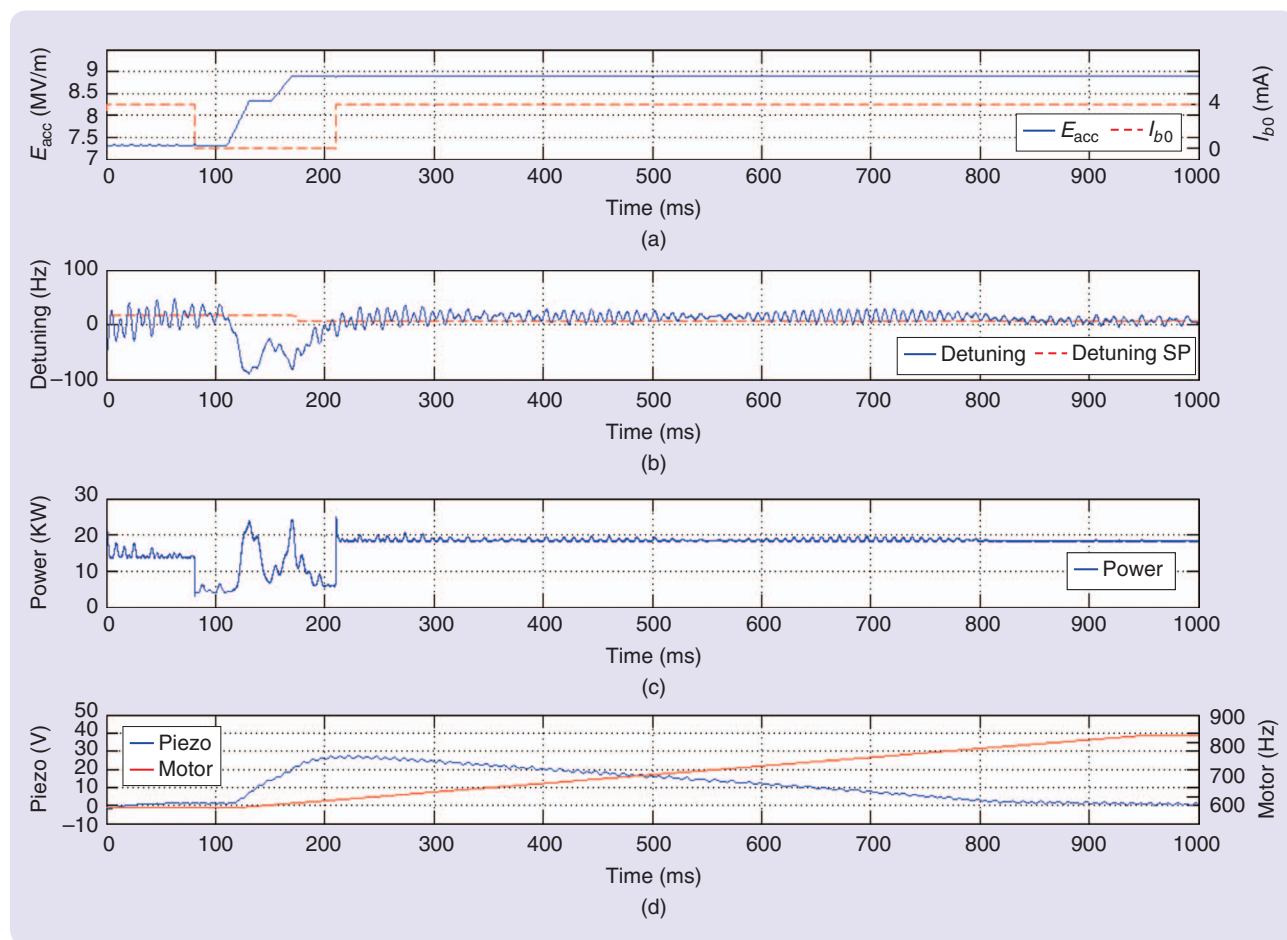


FIGURE 28 Proportional-integral-derivative + Chebyshev filters approach performance. (a) The amplitude of the field inside the cavity throughout the simulation, (b) the cavity’s detuning throughout the simulation, (c) power consumption throughout the simulation, and (d) voltage applied to piezoelectric and motor effect on the cavity detuning.

is switched off at 80 ms [Figure 27(a)] the RF generator power immediately decreases [Figure 27(c)]. Therefore, the consumed power is the power reflected at the cavity entrance and the RF power stored in the cavity. For more details, see “Optimal Frequency Detuning.” Shortly after, the field’s amplitude is increased [Figure 27(a)], causing a decrease in the cavity detuning [Figure 27(b)] due to Lorentz forces. Despite PID compensation acting on the piezo [Figure 27(d)], the drift in the cavity detuning causes the power consumption to rise sharply and saturate at 30 kW [Figure 27(a)]. This causes deviations in the field, as shown in Figure 27(a). Lack of precision on field control is critical, as it has been determined [55] that proper acceleration can be guaranteed with an error smaller than 0.5%. After the transient, once the field’s amplitude has stabilized and the piezo has approached the detuning to its SP, the beam has been switched on again at 220 ms [Figure 27(a)], raising the power consumption [Figure 27(c)]. During the rest of the simulation cavity detuning, deviations from its SP caused by microphonics can be appreciated [Figure 27(b)]. Power consumption increases due to these deviations can also be

observed [Figure 27(c)]. It must finally be noted that, after the transient, the stepper motor, which is a slower actuator than the piezo, starts to tune the cavity, allowing for the piezovoltage (PID control signal) to decrease back to its normal operating band: -5 to 5 V.

PID + Chebyshev Filters Approach

The PID + Chebyshev filters approach, described in [14]–[16], represents a significant enhancement to the control system performance, with respect to the previously considered PID approach. The control strategy used by the PID + Chebyshev filters approach is represented by the block diagram shown in Figure 10.

Figure 28 presents the simulation results obtained by this approach for the same experiment previously considered for the PID approach. Figure 28 has the same chromatic criterion and scaling used for Figure 27. It is observed that the PID + Chebyshev filters approach produces a significant reduction in the detuning oscillations around the SP, which causes a significant drop in power consumption. Although the control performance in the same scenario is

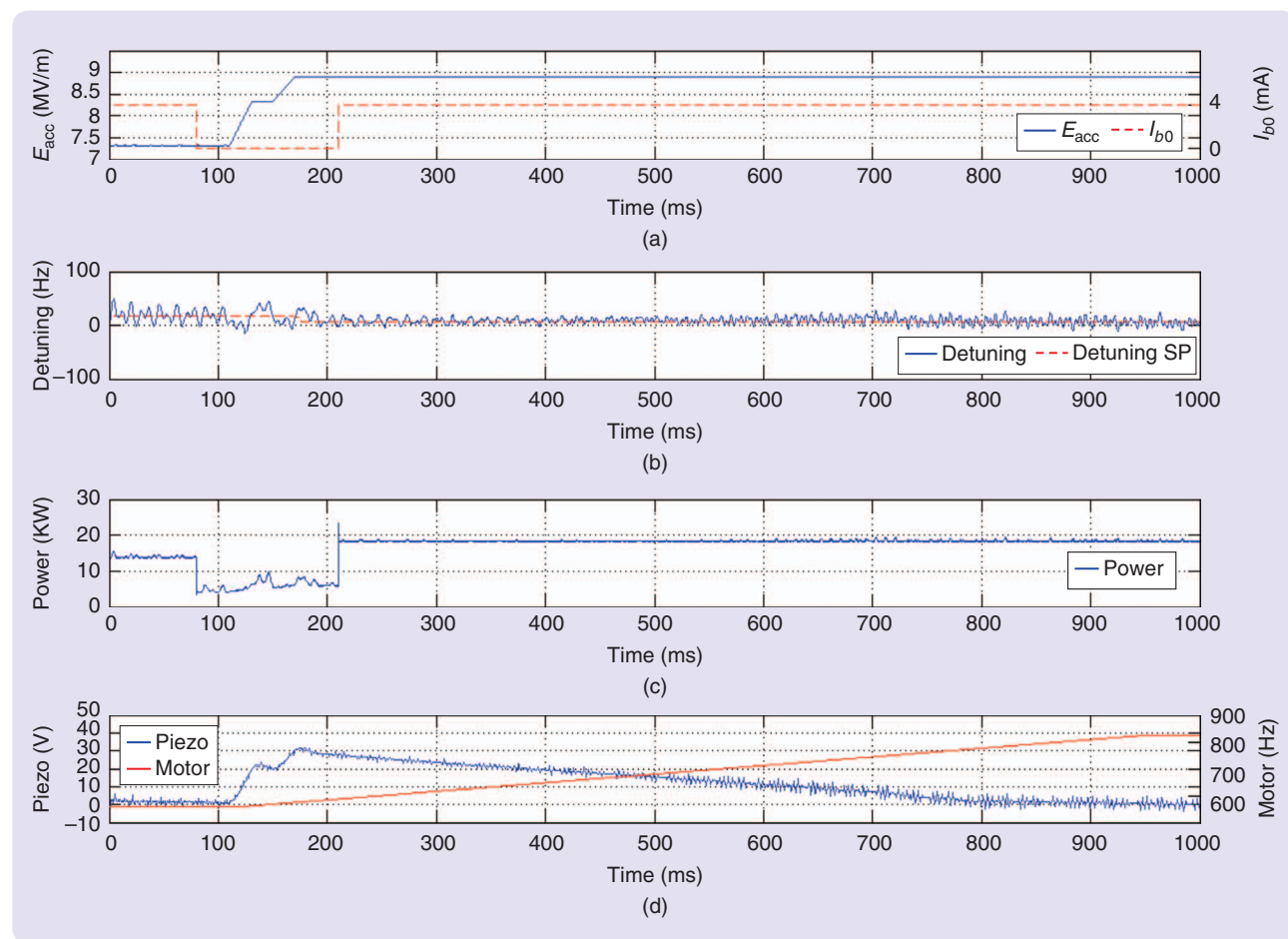


FIGURE 29 Adaptive predictive expert optimized adaptive approach control performance. (a) The amplitude of the field inside the cavity throughout the simulation, (b) the cavity’s detuning throughout the simulation, (c) power consumption throughout the simulation, and (d) voltage applied to piezo and motor effect on the cavity detuning. SP: setpoint.

significantly better, the cavity's detuning experiences a significant deviation from its SP after the cavity failure, due to the growing RF field's amplitude that induces Lorentz forces in the cavity. Furthermore, while the stepper motor is compressing the cavity, an offset between the cavity's detuning and its SP is produced, such that the PID control action cannot compensate. It must be noted that requirements for the maximum control errors on the cavity field control are accomplished (0.5% error on E_{acc} and 0.5° on ϕ_s) with this enhancement.

Optimized Adaptive Control System Approach

Figure 29 presents the simulation results obtained by the ADEX system described by Figure 25, for the same experiment previously considered for the two PID approaches. Figure 29 has the same chromatic criterion and scaling used for Figures 27 and 28. The ADEX system represented in Figure 25 operated with a control period of 2 ms for the AP expert ADEX controller, and an execution time of 200 ms for the notch and Chebyshev filters and the Lorentz forces anticipation block.

The ADEX controller included an adaptive predictive (AP) domain and an upper and lower expert domain. The configuration of the other structure variables of the ADEX controller (for details, see "ADEX Optimized Adaptive Controllers and Systems") was established for the AP domain as follows: 1) the adaptive predictive model was of the second order, with a control period of time delay; 2) the upper and

lower limits on the piezocontrol signal were -30 V and $+50$ V, respectively; 3) no noise level was considered on the cavity frequency detuning; 4) the rate of change per control period of the desired process output trajectory was equal to 100 Hz; and 5) the prediction horizon was equal to five control periods. The ADEX controller upper and lower expert domains determined an expert control action for the piezo when the frequency detuning surpassed the upper level of 300 Hz or under passed the lower level of -100 Hz.

To make a qualitative comparison between the results obtained with the ADEX system and the PID-based system, Figure 30 integrates results from simulations recorded in Figures 28 and 29. Figure 30(a) shows the cavity detuning in both experiences and their SPs. The detuning under ADEX system control is represented by the green line, while the PID + Chebyshev filters was shown in blue. The SPs of both are represented by the red line. Figure 30(b) shows power consumption under ADEX system control, represented by the green line, while the power consumption under PID-based system control is shown in blue. The following remarks can be derived from a comparative analysis using Figure 30. First, a significant reduction in the cavity detuning oscillations around their SP has been achieved by the ADEX system, while the power consumption was reduced and is maintained nearly at its minimum throughout the experiment. Second, the offset between the cavity detuning and its SP observed under the PID-based system practically disappears under the ADEX system.

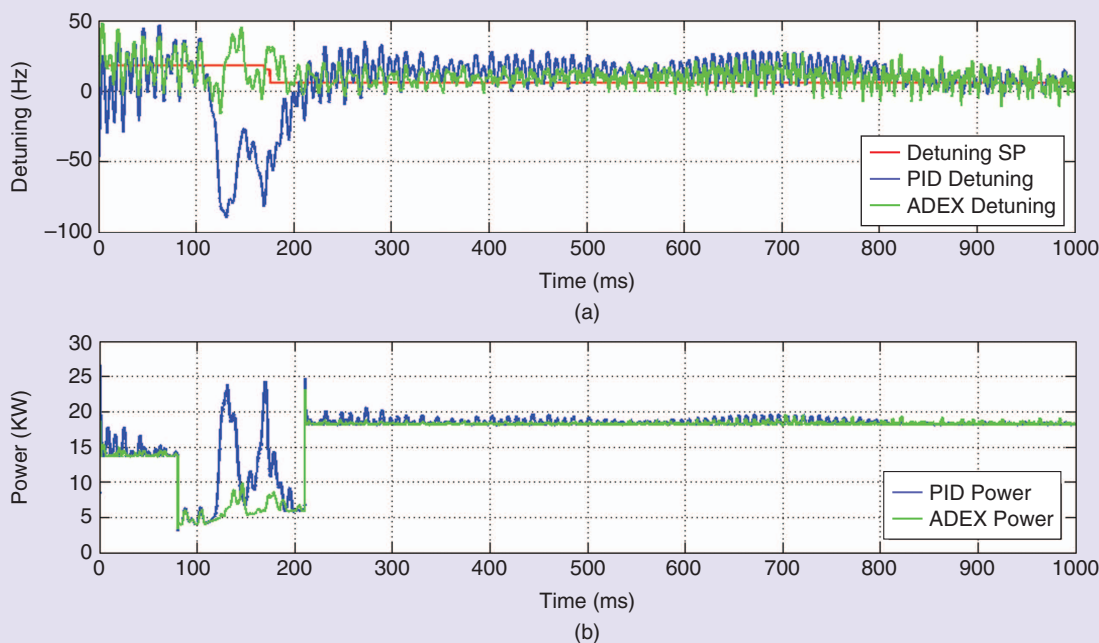


FIGURE 30 Adaptive predictive expert (ADEX) and proportional-integral-derivative- (PID)-based systems detuning control performance. (a) ADEX and PID-based systems detuning control performance and (b) ADEX and PID-based systems power consumption throughout the simulation. SP: setpoint.

In this experiment, the ADEX system exhibited more reliability than the PID-based system in an uncertain scenario with unforeseen perturbations.

Perturbation in the Simulated Scenario for Reliability Analysis

In this section, a perturbed simulated scenario (PSS) will be applied to the cavity both under the PID-based control system with Chebyshev filters and the ADEX system to comparatively analyze the performance of both methodologies for a reliability analysis. The PSS is equivalent to the previously described scenario. However, an unforeseen microphonic perturbation of 20-Hz frequency occurs with a detuning amplitude of 50 Hz on the cavity RF resonance frequency. The results obtained by the execution of the PSS under the PID-based system control are presented in Figure 31.

Figure 31 is similar to Figure 26, until the beam is turned on after the variables are stabilized in the simulated scenario [Figure 31(a)]. Thus, the explanation of the evolution of

the cavity variables in Figure 31 up to this point is the same as that presented for Figure 28. However, immediately after the beam has been switched on and the unforeseen external microphonic perturbation is simulated in the system at approximately 220 ms, strong cyclical oscillations can be observed in the cavity's detuning [Figure 31(b)]. These oscillations are hardly compensated by the voltage that the PID is applying to the piezoelectric actuator [Figure 31(d)] and the drifts of the frequency from its SP cause the power [Figure 31(c)] to increase even more, approaching the limit of power supply (30.000 W) three times (270, 320, and 400 ms). The third time the power supply reaches saturation, the RF control system loses control of the cavity and the field drops [Figure 31(a)]. The simulation was interrupted at 410 ms, while it was intended to last 1 s.

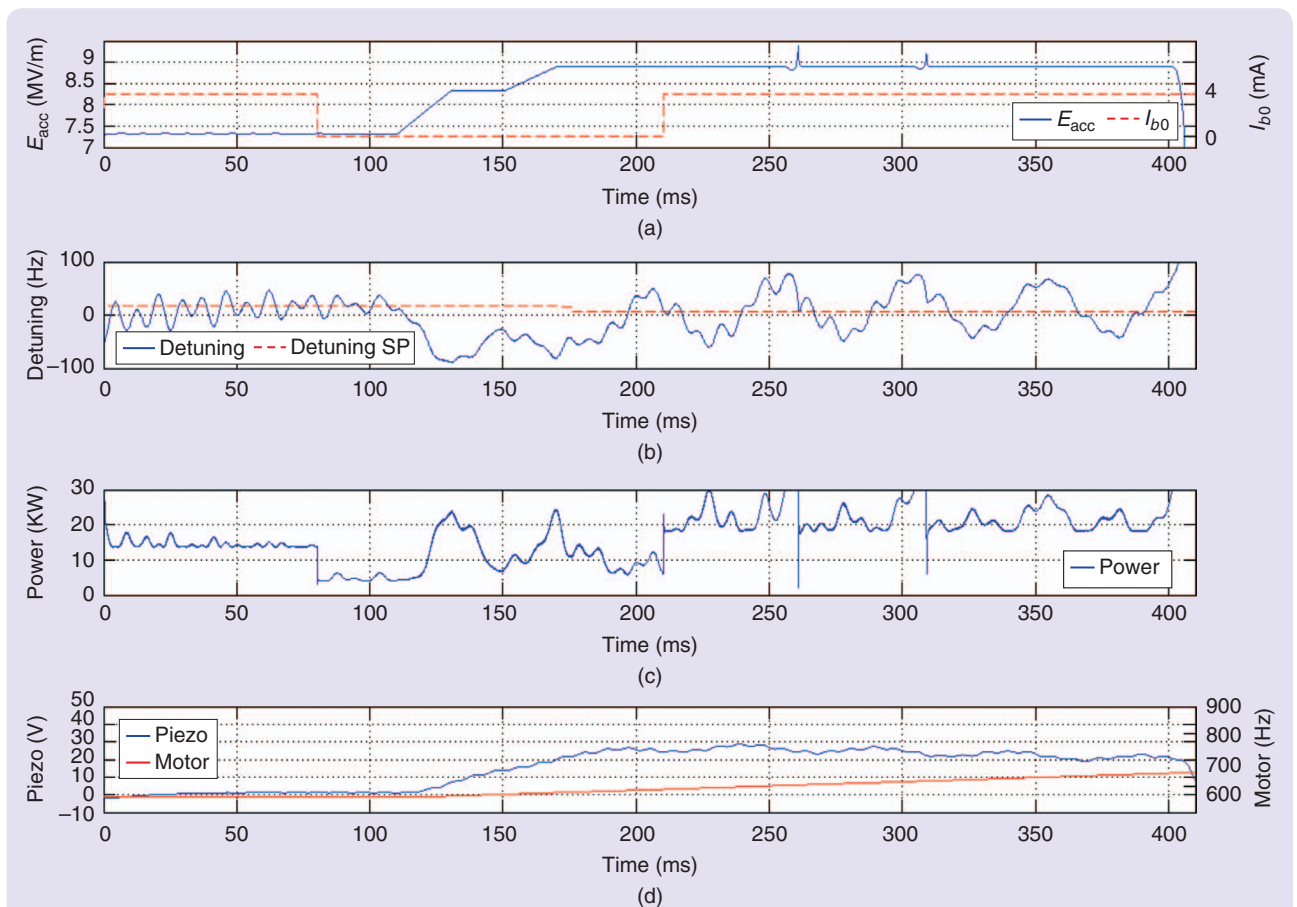


FIGURE 31 Proportional-integral-derivative- (PID)-based system performance under unexpected strong perturbations. (a) The amplitude of the field inside the cavity throughout the simulation, (b) the cavity's detuning throughout the simulation, (c) power consumption throughout the simulation, and (d) voltage applied to piezo and motor effect on the cavity detuning. SP: setpoint.

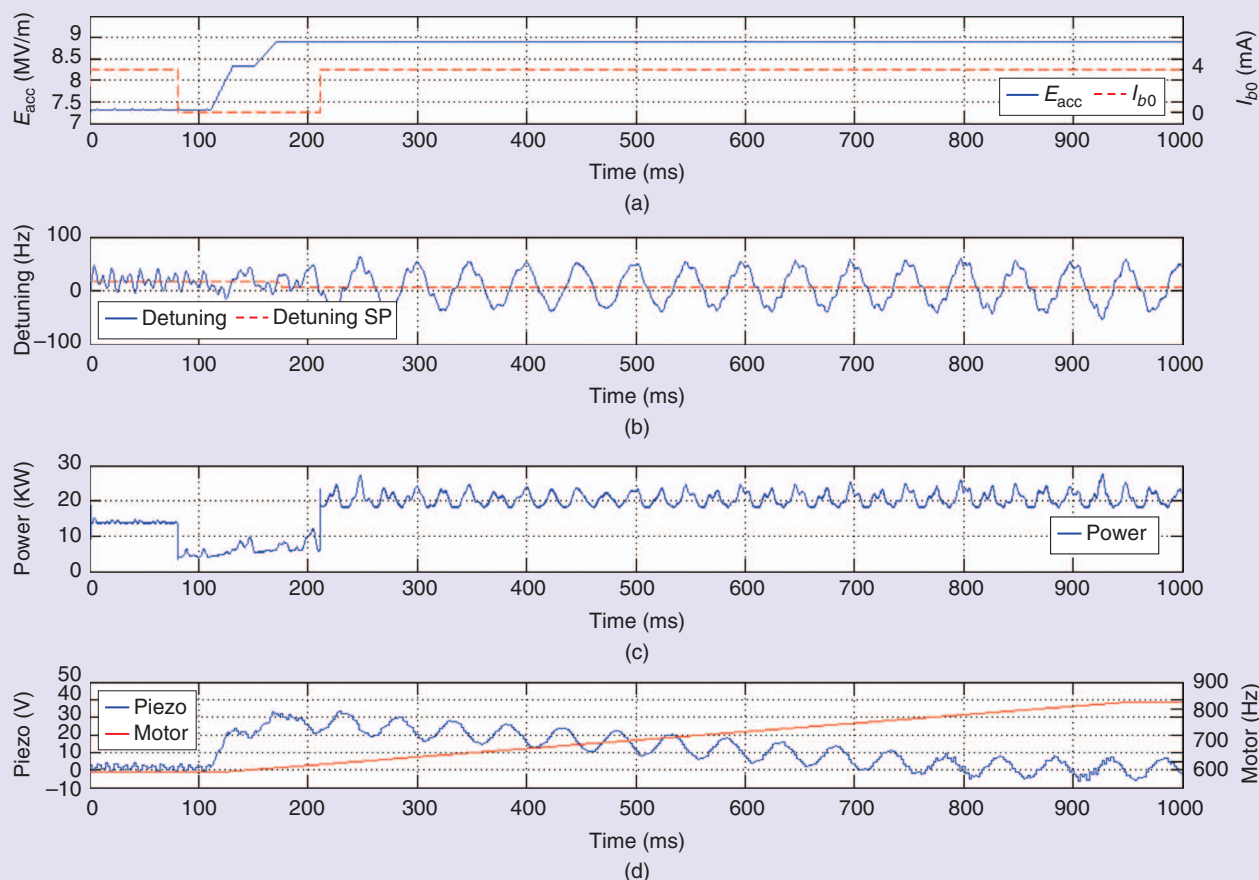


FIGURE 32 Adaptive predictive expert system (ADEX) performance under unexpected strong perturbations. (a) The amplitude of the field inside the cavity throughout the simulation, (b) the cavity's detuning throughout the simulation, (c) power consumption throughout the simulation, and (d) voltage applied to piezo and motor effect on the cavity detuning.

The results obtained by the execution of the PSS under the ADEX system control are presented in Figure 32. This figure is similar to Figure 29, until the beam is turned on after the cavity variables are stabilized [Figure 32(a)]. Thus, the evolution of the cavity variables in Figure 32 up to this point is equivalent to that presented in Figure 29. However, right after the beam has been switched on and the unforeseen external microphonics perturbation is introduced in the simulation at approximately 220 ms, strong cyclical oscillations can be observed in the cavity's detuning [Figure 32(b)]. However, the resonance frequency was maintained within operational limits and without the RF system losing control of the field inside the cavity. It can also be observed that the power consumption [Figure 32(c)] and the control action on the piezo [Figure 32(d)] evolved with limited oscillations around the values previously observed in Figure 29, where the strong perturbation was not present.

In this experiment, the ADEX system exhibited more reliability than the PID-based system in an uncertain scenario with unforeseen perturbations. The PID control parameters that were tuned for the foreseen operating conditions in a

context of certainty failed to maintain control over the critical variables of the process when an unforeseen perturbation changed the process dynamics. On the other hand, the ADEX system used its adaptive capacity to identify the changing process dynamics introduced by the unforeseen perturbation and self-tune its parameters in real time to minimize the impact of the perturbation. This maintained the cavity in operation.

CONCLUSIONS

This article describes an ADS, the acceleration process that occurs in an SC cavity of a linac, and the complex environment in which this process operates. This acceleration process is subject to detrimental mechanical vibration, severe time constraints, perturbations (such as microphonics and Lorentz forces), and a time-varying environment that changes its dynamics, depending on the operating conditions. The need for precise control of this acceleration process cannot be overemphasized since it will determine satisfactory operation of the linac and the operational availability of the entire ADS.

The need for precise control of this acceleration process cannot be overemphasized since it will determine satisfactory operation of the linac and the operational availability of the entire ADS.

A CNRS simulator of a 704.4-MHz SC cavity was used to comparatively evaluate the control performance of an ADEX-optimized adaptive control system and alternative PID-based control systems, as applied to the control of the CTS loop of the cavity. The CTS loop controls the cavity frequency detuning. Its performance determines the energy required by the LLRF loop for proper operation of the cavity and its operational capacity under certain scenarios, such as an adjacent cavity failure requiring application of the local compensation method or the presence of unforeseen perturbations. The high reliability demanded by linac operation necessitates optimized and stable control performance of the CTS loop in all process environments where cavity operation is physically possible.

The article describes, in detail, the control strategies used in the previous PID-based control solutions that were applied to the CTS loop and the OCS used in the ADEX system. Notch filters were introduced in the definition of the OCS that, in addition to ADEX controllers, also integrated Chebyshev filters and anticipation of the effects of Lorentz forces when power variations occurred in the cavity field. In this way, the OCS gathered the tools to attenuate the excitation of the cavity's resonance modes by the ADEX controller's actions, minimized the known microphonics induced by external perturbations, and compensated in advance for Lorentz forces.

The experimental results in simulation proved the efficiency of the LLRF control loop, under PID control, and the CTS control loop, under PID and ADEX control, working together but independently in a standard, simulated scenario. The comparative analysis of the results show, in this simulation scenario, that the ADEX system reduced the frequency-detuning deviations from its SP, while power consumption was maintained nearly at its minimum. In a second scenario, an unforeseen external microphonic perturbation of 20-Hz frequency, which caused oscillations with an amplitude of 50 Hz in the frequency detuning, was applied to the cavity simulator. This unforeseen perturbation caused the loss of control of the cavity under PID control. Under ADEX control, a much more aggressive control action maintained the resonance frequency within operational limits and the field inside the cavity under control by the LLRF system.

These simulation results show how fixed-parameter control/command systems, designed in a context of certainty, where it is assumed that the process dynamics and

perturbations acting on the process are correctly modeled and known, can deteriorate their performance when uncertainties are introduced in the operating context. On the other hand, ADEX OACS needs no accurate knowledge of the process dynamics, its changes with time, or perturbations acting on the process and can handle uncertainty and unknown perturbations while maintaining desired performance, as this simulation showed.

AUTHOR INFORMATION

Isaías Martín-Hoyo (imhoyo@gmail.com) is an industrial engineer from the Technical University of Madrid. He received the master's degree in electric, electronic, and control engineering from the Universidad Nacional de Educación a Distancia, where he is currently pursuing a Ph.D. degree. He has more than five years of professional experience in the area of industrial optimized adaptive control and developed and implemented optimized adaptive control systems currently used for the production of composite parts of Airbus airplanes A350 and A380. He developed optimized adaptive control systems for the nuclear domain, participating in Task 3.6 "Instrumentation and Control" of the EU FP7 CDT project and was responsible for the development of Task 3.2 "Experimental evaluation of ADEX control on a 700 MHz prototypical cryomodule" of the EU FP7 MAX project. He has published and presented several articles in indexed journals and international conferences. He can be contacted at Plaza Valle de la Jara s/n77, CP 28035, Madrid.

Frédéric Bouly is an accelerator physicist at the National Institute of Nuclear and Particle Physics (IN2P3), French National Center for Scientific Research. He received the bachelor's degree in nuclear and reactors physics from the Grenoble Institute of Technology in 2008, the M.S. degree in energetic physics, with a specialization in accelerator physics from the Joint Universities Accelerator School, and the Ph.D. degree in 2011 from the Université Paris Sud XI. In 2012, he worked at the European Organization for Nuclear Research on beam dynamics studies for the High-Luminosity LHC project. Since 2013, he has been a researcher at the Laboratory of Subatomic Physics and Cosmology, where his main activities are dedicated to theoretical and experimental beam physics studies in hadrons accelerators. He is responsible for the MYRRHA accelerator research and development activities being implemented at IN2P3.

Nicolas Gandolfo obtained the master's degree in mechatronics engineering from the Institut des Sciences et Techniques

des Yvelines. He currently works as a research engineer at the Centre National de la Recherche Scientifique in the accelerator division of the Institut de Physique Nucléaire d'Orsay. He has over ten years of experience in the field of superconducting resonators for particle accelerators. His technical background is focused on the mechanical design and automatic control of motorized systems intended to work under low temperatures, vacuums, and high-radiation environments. He has published and contributed to several articles in international conferences about particle accelerators.

Christophe Joly is a radio-frequency research engineer with the Accelerator Research Department of the Institut de Physique Nucléaire d'Orsay, where he is in charge of the Accelerator Electronics group and responsible for the MYRRHA project. He joined Centre National de la Recherche Scientifique in 1996, in the framework of the international project LHC, to work on the development of the calibration system for the 6000 thermometers necessary for the accelerator. Since 2001, he has developed various RF systems, in particular the low-level radio frequency (LLRF) feedback systems for the research and development on the superconducting cavities in the framework of IPHI, SPIRAL2, EUROTRANS, and MAX projects. He graduated from the INFOTEP Engineer School, Pierre and Marie Curie University, in 2004. His main activity is the research and development of digital LLRF feedback systems. He is also involved in RF power developments, such as the French contribution (RF power chain for pLinac) to the FAIR project.

Rocco Paparella is a physicist from the University of Milan, Italy, where he obtained the Ph.D. degree in physics, astrophysics, and applied physics in 2008. He works as a junior researcher at the LASA Laboratory, Italian Institute of Nuclear Physics, Milan. He initially focused on control systems techniques for particle accelerators. His studies were extended to superconducting resonators production, qualification, and tune control in the framework of several international projects such as the International Linear Collider, European-XFEL free-electron laser, European Spallation Source, and PDS-XADS/EUROTRANS/MYRRHA ADSs for nuclear-waste transmutation.

Jean-Luc Biarrotte is a particle accelerator physicist and scientific director of the National Institute of Nuclear and Particle Physics, French National Center for Scientific Research (CNRS), where, since April 2016, he has been in charge of accelerators and technologies. He was head of the Modeling and Simulation team in the Accelerator Research Department, Institut de Physique Nucléaire d'Orsay. He graduated from the Ecole Nationale Supérieure de Physique de Grenoble in 1995 and joined CNRS in 2000 after obtaining the Ph.D. at CEA Saclay/University Paris-Sud. His expertise is the design of high-power superconducting linear accelerators for hadron-beam-based nuclear physics. He was the CNRS coordinator for the ADS accelerators

activities and involved in the MYRRHA project, in which he coordinated with the MAX EURATOM FP7 project from 2011 to 2014. He has been involved in the IPHI, EURISOL, and EUROTRANS (previously PDS-XADS) projects and the SPIRAL-2 project at GANIL. In 2009, he was awarded the J-Louis Laclare Prize from Société Française de Physique.

Juan M. Martín-Sánchez received the industrial engineer degree in 1970 and the doctor industrial engineer degree in 1974, both from the Polytechnic University of Catalunya, Spain. He is currently a professor at the Open University of Spain. From 1971 to 1976, his research activities continued at Grenoble and Toulouse Universities, France; the MIT Draper Laboratory, United States; and the University of Alberta (U of A), Canada. In 1976, he filed the first patent for predictive and adaptive predictive control and subsequently obtained five additional patents on these methodologies. From 1981 to 1986, he was a professor and research fellow of the Natural Sciences and Engineering Research Council of Canada, U of A. Between 1986 and 1998, he was president of SCAP Europa. In 1999, he founded ADEX S.L. He has authored more than 100 publications and four books on adaptive predictive control, including *Adex Optimized Adaptive Controllers and Systems: From Research to Industrial Practice* (Springer, 2015). From 2004 to 2009, he was president of the IEEE Joint Spanish Chapter of the IEEE Industry Applications Society and IEEE Control Systems Society, which organized the biannual Seminar of Advanced Industrial Control Applications. He is a Fellow of the IEEE.

REFERENCES

- [1] World Energy Outlook. (2014, Nov.). *World Energy Outlook*. Paris. [Online]. Available: <http://www.worldenergyoutlook.org/weo2014/>
- [2] NEA/OECD. (2012, Nov.). *Nuclear Energy Today*, 2nd ed. [Online]. Available: <http://www.oecd-nea.org/pub/nuclearenergytoday/6885-nuclear-energy-today.pdf>
- [3] D. Struwe and J. Somers. (2008, Oct.). Overview of activities in Europe exploring options for transmutation. NUKLEAR, JRC-ITU, Karlsruhe, Germany. [Online]. Available: http://cordis.europa.eu/pub/fp7/fission/docs/euradwaste-2008-presentations/session-5/3_pres_struwe/overview_of_activities_in_europe.pdf
- [4] E. M. G. Romero. (2007, Mar.). Rational and added value of P&T for waste management policies. Project PATEROS, Sixth Framework Programme, Work Package 1, Deliverable 1.1, Karlsruhe, Germany, Research and Training on Nuclear Energy, Coordination action. [Online]. Available: <http://pateros.sckcen.be/en/Deliverables>
- [5] P&T European Roadmap for sustainable nuclear energy (PARTEROS). Tech. Rep. FP6-036418. [Online]. Available: <http://pateros.sckcen.be/en>
- [6] EUROpean Research Programme for the TRANsmutation of high level nuclear waste in an accelerator driven system (EUROTRANS). Tech. Rep. FI6W-CT-2004-516520. [Online]. Available: http://cordis.europa.eu/project/rcn/85226_es.html
- [7] EUROpean research programme for the PARTitioning of minor actinides and some long-lived fission products from high active wastes issuing the reprocessing of spent nuclear fuels (EUROPART). Tech. Rep. FI6W-CT-2003-508854. [Online]. Available: http://cordis.europa.eu/project/rcn/74122_en.html
- [8] Preliminary design studies of an eXperimental accelerator-driven system (PDS-XADS). Tech. Rep. FIKW-CT-2001-00179. [Online]. Available: http://cordis.europa.eu/project/rcn/58635_en.html
- [9] MYRRHA accelerator eXperiment, research & development programme (MAX). Tech. Rep. 269565. [Online]. Available: http://cordis.europa.eu/result/rcn/54795_en.html

- [10] T. Kandil, H. Khalil, J. Vincent, T. Grimm, W. Hartung, J. Popielarski, R. York, and S. Seshagiri, "Adaptive feedforward cancellation of sinusoidal disturbances in superconducting RF cavities," *Nucl. Instrum. Methods Phys. Res. A*, vol. 550, pp. 514–520, 2005.
- [11] A. Neumann, W. Anders, S. Klauke, J. Knobloch, O. Kugeler, and M. Schuster, "Characterization of a piezo-based microphonics compensation system at Hobocat," in *Proc. European Particle Accelerator Conf.*, Edinburgh, Scotland, 2006, pp. 408–410.
- [12] A. Neumann. (2008, July). Compensating microphonics in SRF cavities to ensure beam stability for future free-electron-lasers. Ph.D. dissertation, Humboldt-Universität zu Berlin, Berlin. [Online]. Available: <https://edoc.hu-berlin.de/bitstream/handle/18452/16500/neumann.pdf?sequence=1&isAllowed=y>
- [13] T. Grimm, W. Hartung, T. Kandil, H. Khalil, J. Popielarski, C. Radcliffe, J. Vincent, and R. York, "Measurement and control of microphonics in high loaded-q superconducting RF cavities," in *Proc. Linear Accelerator Conf.*, Lubbeck, Germany, 2004, pp. 763–765.
- [14] M. Luong. (2007, Oct.). Microphonics analysis and compensation with a feedback loop at low cavity gradient. Commissariat l'nergie Atomique. [Online]. Available: <http://irfu.cea.fr/Phoceia/file.php?class=std&&file=Doc/Publications/Archives/dapnia-07-185.pdf>
- [15] F. Bouly, J. L. Biarrotte, and C. Joly, "Low level radio-frequency developments toward a fault-tolerant linac scheme for an accelerator driven system," in *Proc. XXV Int. Linear Accelerator Conf.*, Tsukuba, Japan, 2010, pp. 244–246.
- [16] F. Bouly. (2011, Nov.). Etude d'un module accélérateur et de ses systèmes de régulation pour le projet MYRRHA. Ph.D. dissertation, Université Paris Sud, Paris XI. [Online]. Available: https://tel.archives-ouvertes.fr/tel-00660392/file/VA2_BOULY_Frederic_03112011.pdf
- [17] G. Devanz, P. Bosland, M. Desmons, E. Jacques, M. Luong, and B. Visentin, "Compensation of Lorentz force detuning of a TTF 9-cell cavity with a new integrated piezo tuner," in *Proc. European Particle Accelerator Conf.*, Edinburgh, UK, 2006, pp. 378–380.
- [18] J. M. Martín-Sánchez. (2003). Adaptive predictive expert control system. U.S. Patent PCT/IB00/01 368. [Online]. Available: <http://www.adexcop.com/archivos/Patente%20EEUU%202003.pdf>
- [19] J. M. Martín-Sánchez and J. Rodellar, *ADEX Optimized Adaptive Controllers and Systems: From Research to Industrial Practice*. New York: Springer, 2015.
- [20] A. Nevado, I. Martín-Hoyo, and F. Mur, "Design and application of a steam temperature optimizer in a combined cycle," *Int. J. Adapt. Control Signal Process.*, vol. 26, no. 10, pp. 919–931, 2012.
- [21] R. Estrada, A. Favela, A. Nevado, A. Raimondi, and E. Gracia, "Control of five sulphur recovery units at PEMEX cadereyta refinery," in *Proc. 3rd IEEE Seminar Advanced Industrial Control Applications*, Madrid, Spain, 2009, pp. 79–88.
- [22] A. Nevado, I. Martín-Hoyo, and R. Requena, "ADEX control of steam temperature in a combined cycle," in *Proc. IEEE Int. Energy Conf.*, Manama, Bahrain, 2010, pp. 137–142.
- [23] R. Pérez, A. Geddes, and A. Clegg, "Adaptive predictive expert control of superheated steam temperature in a coal-fired power plant," *Int. J. Adapt. Control Signal Process.*, vol. 26, no. 10, pp. 932–944, 2012.
- [24] J. M. Martín-Sánchez. (1976). Adaptive predictive control system. U.S. Patent 4 197 576. [Online]. Available: <http://www.adexcop.com/archivos/PatenteEEUU1980.pdf>
- [25] J. M. Martín-Sánchez and J. Rodellar, *Adaptive Predictive Control: From the Concepts to Plant Optimization*. Englewood Cliffs, NJ: Prentice Hall, 1996.
- [26] J. M. Martín-Sánchez, J. M. Lemos, and J. Rodellar, "Survey of industrial optimized adaptive control," *Int. J. Adapt. Control Signal Process.*, vol. 26, no. 10, pp. 881–918, 2012.
- [27] J. L. Biarrotte, M. E. Yakoubi, F. Chatelet, N. Gandolfo, C. Joly, J. Lesrel, H. Sagnac, A. Bosotti, R. Paparella, P. Pierini, F. Bouly, and I. Martín-Hoyo, "Commissioning of the max 700 MHz test stand," in *Proc. 27th Linear Accelerator Conf.*, Geneva, Switzerland, 2014, pp. 610–612.
- [28] G. V. Tuyle, M. Todosow, A. Aronson, H. Takahashi, and M. Geiger, "Accelerator driven sub-critical target concept for transmutation of nuclear wastes," *Nucl. Technol.*, vol. 101, no. 1, pp. 1–17, 1993.
- [29] B. Boullis, "Long-lived radionuclides partitioned at will," *Clefs CEA*, vol. 34, no. 46, pp. 18–23, 2002.
- [30] A. Zaetta, "Transmutation is technically feasible," *Clefs CEA*, vol. 34, no. 46, pp. 32–39, 2002.
- [31] The MYRRHA website. [Online]. Available: <http://myrrha.sckcen.be/>
- [32] G. Rimpault, P. Darde, F. Mellier, R. Dagan, M. Schikorr, A. Weisenburger, D. Maes, V. Sobolev, B. Arien, D. Lamberts, D. De Bruyn, A. C. Mueller, and J. L. Biarrotte, "The issue of accelerator beam trips for efficient ADS operation," in *Nucl. Technol.*, vol. 184, no. 2, pp. 249–260, 2013.
- [33] D. Vandeplassche and L. Medeiros Romao. (2012). Accelerator driven systems, in *Proc. Int. Particle Accelerator Conf.*, New Orleans, LA, 2012, pp. 6–10.
- [34] The MAX website. [Online]. Available: <http://ipnwww.in2p3.fr/MAX/>
- [35] R. Salemme, F. Bouly, L. Medeiros Romao, D. Vandeplassche, J. L. Biarrotte, M. Baylac, D. Bondoux, J. M. De Conto, E. Froidefond, and D. Uriot, "Design progress of the MYRRHA low energy beam line," in *Proc. Linear Accelerator*, Geneva, Switzerland, 2014, pp. 381–383.
- [36] D. Mäder, M. Basten, D. Koser, H. C. Lenz, N. F. Petry, H. Podlech, A. Schempp, M. Schwarz, M. Vossberg, and C. Zhang, "R&D of the 17 MeV MYRRHA injector," in *Proc. Linear Accelerator*, Geneva, Switzerland, 2014, pp. 202–204.
- [37] J. L. Biarrotte, S. Bousson, T. Junquera, A. C. Mueller, and A. Olivier, "A reference accelerator scheme for ADS applications," *Nucl. Instrum. Methods Phys. Res. A*, vol. 562, no. 2, pp. 656–661, 2006.
- [38] H. Sagnac, J. L. Biarrotte, S. Blivet, P. Duchesne, N. Gandolfo, J. Lesrel, G. Olry, E. Rampoux, and D. Reynet, "The MYRRHA spoke cryomodule design," in *Proc. Linear Accelerator*, Geneva, Switzerland, 2014, pp. 613–615.
- [39] F. Bouly, A. Bosotti, R. Paparella, P. Pierini, J. L. Biarrotte, S. Berthelot, M. El Yakoubi, C. Joly, J. Lesrel, and E. Rampoux, "Developments and tests of a 700 MHz cryomodule for the superconducting linac of MYRRHA," in *Proc. 16th Int. Conf. RF Superconductivity*, Paris, France, 2013, pp. 250–254.
- [40] J. L. Biarrotte, D. Uriot, F. Bouly, J. P. Carneiro, and D. Vandeplassche, "Design of the MYRRHA 17-600 MeV superconducting linac," in *Proc. 16th Int. Conf. RF Superconductivity*, Paris, France, 2013, pp. 129–132.
- [41] J. L. Biarrotte, M. Novati, P. Pierini, H. Safa, and D. Uriot, "Beam dynamics studies for the fault tolerance assessment of the PDS-XADS linac," in *Proc. European Physical Society Accelerator*, Lucerne, Switzerland, 2004, pp. 1282–1284.
- [42] L. Burgazzi and P. Pierini, "Reliability studies of a high-power proton accelerator for accelerator-driven system applications for nuclear waste transmutation," *Rel. Eng. Syst. Saf.*, vol. 92, no. 4, pp. 449–463, 2007.
- [43] F. Bouly, J. L. Biarrotte, and D. Uriot, "Fault tolerance and consequences in the MYRRHA superconducting linac," in *Proc. Linear Accelerator*, Geneva, Switzerland, 2014, pp. 297–299.
- [44] A. Bosotti, C. Pagani, P. Pierini, J. P. Charrier, B. Visentin, G. Ciovati, and P. Kneisel, "RF tests of the beta = 0.5 five cell TRASCO cavities," in *Proc. European Physical Society Accelerator*, Lucerne, Switzerland, 2004, pp. 1024–1026.
- [45] J. C. Slater, "Microwave electronics," *Rev. Mod. Phys.*, vol. 18, no. 4, pp. 441–512, 1946.
- [46] J. M. Martín-Sánchez. (1980). Adaptive predictive control system. U.S. Patent 4 358 822. [Online]. Available: <http://www.adexcop.com/archivos/Patente%20EEUU%201982.pdf>
- [47] R. M. De Keyser, P. G. Van de Velde, F. A. Dumoriter, "A comparative study of self-adaptive long-range predictive control methods," in *Proc. 7th IFAC Symp. Identification and Control*, York, UK, 1985, pp. 1317–1322.
- [48] D. Clarke and C. Mohtadi, "Properties of generalized predictive control," in *Proc. 10th IFAC World Congr.*, Munich, Germany, 1987, pp. 63–74.
- [49] J. Rodellar, "Optimal design of the driver block in the adaptive predictive control system," Ph.D. dissertation, Univ. Barcelona, Barcelona, Oct. 1985.
- [50] J. M. Martín-Sánchez and S. L. Shah, "Multivariable adaptive predictive control of a binary distillation column," *Automatica*, vol. 20, no. 5, pp. 607–620, 1984.
- [51] J. M. Martín-Sánchez, "A globally stable APCS in the presence of bounded unmeasured noises and disturbances," in *Proc. 21st IEEE Conf. Decision and Control*, Orlando, 1982, pp. 761–769.
- [52] J. M. Martín-Sánchez, S. L. Shah, and D. G. Fisher, "A stable adaptive predictive control system," *Int. J. Control*, vol. 39, no. 1, pp. 215–234, 1984.
- [53] J. M. Martín-Sánchez, "A new solution to adaptive control," *Proc. IEEE*, vol. 64, no. 8, pp. 1209–1218, Aug. 1976.
- [54] OPC foundation. [Online]. Available: <https://opcfoundation.org/>
- [55] A. Mosnier. (2002). Control of SRF cavities in high power proton linac, in *Proc. European Physical Society Accelerator*, Paris, France. [Online]. Available: <http://irfu.cea.fr/Phoceia/file.php?class=std&&file=Doc/Publications/Archives/dapnia-02-190.pdf>

